Copy 5

NASA TM X-696

NASA TM X-696

TECHNICAL MEMORANDUM

X-696

TRANSONIC AERODYNAMIC CHARACTERISTICS OF A HORIZONTAL-TAKE-OFF-AND-HORIZONTAL-LANDING RECOVERABLE-BOOSTER CONCEPT WITH UPPER STAGES ARRANGED IN PARALLEL

By P. Kenneth Pierpont

Langley Research Center
Langley Station, Hampton, Va.

NATIONAL AERONAUTICS AND SPACE ADMINISTRATION

WASHINGTON

August 1962

NATIONAL AERONAUTICS AND SPACE ADMINISTRATION

TECHNICAL MEMORANDUM X-696 [redacted]

TRANSONIC AERODYNAMIC CHARACTERISTICS OF A HORIZONTAL-TAKE-OFF-AND-HORIZONTAL-LANDING RECOVERABLE-BOOSTER CONCEPT WITH UPPER STAGES ARRANGED IN PARALLEL*

By P. Kenneth Pierpont

SUMMARY

A transonic investigation has been made of a preliminary concept of a horizontal-take-off-and-horizontal-landing recoverable first-stage booster with various large upper stages. The recoverable booster consisted of a wedge-slab 70° delta wing with a semicylindrical fuselage. The upper stages consisted of either a one-stage or a two-stage expendable rocket booster and a ballistic, rocket, or winged-rocket spacecraft. The upper stages were tested in both piggyback and underslung positions on both a high-wing and a low-wing recoverable booster. The tests were made in the 8-foot transonic pressure tunnel over a Mach number range from 0.6 to 1.2. Data were obtained at 0° and 5° sideslip over an angle-of-attack range from -2° to 12°. The Reynolds number per foot varied from 1.6×10^6 to 3.2×10^6.

The results showed that only small changes in longitudinal stability and trim occurred when either the one-stage or two-stage rocket booster was added to the recoverable booster. However, the installation of upper stages to the recoverable booster caused a significant reduction in the directional stability. An increase of as much as 50 percent in transonic drag was attributable to the upper stages, but improvement in the drag could be achieved by closing the afterbody. The one-stage rocket booster caused a larger transonic drag rise than the two-stage rocket booster because of the adverse effect on the overall area distribution. Neither high-wing nor low-wing arrangements offered distinct advantages in stability or drag.

*Title, Unclassified.

INTRODUCTION

Some of the anticipated advantages of placing large payloads in earth orbit through the use of a vertical-take-off-and-horizontal-landing (VTOHL) recoverable-booster system have been outlined in reference 1, and the transonic aerodynamic characteristics of a VTOHL recoverable booster were reported therein. An alternate approach to the recoverable booster consists of using a manned horizontal-take-off-and-horizontal-landing (HTOHL) vehicle as first stage, and mounting the upper stages in parallel with the first stage. Such a booster, if propelled by air-ingestion engines, offers the following capabilities in addition to those indicated in reference 1: offset launch capability through the use of aerodynamic flight to the required orbit plane; ferry flight of the launch vehicle, and possibly of upper-stage elements; piloted control of both launch altitude and attitude; large diversity of upper-stage configurations; normal development and testing of the first stage throughout its flight envelope; and growth potential. A principal advantage of the HTOHL recoverable-booster system lies in its inherent high aerodynamic efficiency.

A program of investigation to determine the aerodynamic characteristics of horizontal-take-off-and-horizontal-landing recoverable-booster concepts has, therefore, been undertaken at transonic and hypersonic speeds. The present paper contains results for several preliminary configurations investigated at transonic speeds. Results of tests of the first-stage recoverable booster alone were reported in reference 2. For the present investigation, the upper stages consisted of several rocket boosters and spacecraft mounted in parallel with the winged recoverable booster. Mission requirements were established to place a maximum of approximately 30,000 pounds of spacecraft into a 300-nautical-mile orbit. As indicated in reference 2, the first stage was conceived to utilize turboramjet power plants with the hydrocarbon fuel carried entirely within the fuselage. First-stage separation was estimated to occur at a Mach number of 6.0 and an altitude of about 100,000 feet, with the upper stages sized for the specific mission. Gross take-off wing loading was assumed to be 120 lb/sq ft and the ratio of thrust to gross weight was assumed to be 0.60. The resultant landing wing loading for the recoverable booster was approximately 40 lb/sq ft. With the above assumptions, the models tested were approximately 1/50 scale. The purpose of the investigation is to provide preliminary aerodynamic information to assist in the evaluation of the technical feasibility of the recoverable-booster concept.

Data were obtained over a range of angles of attack from -2° to 12°. A few data were obtained at a sideslip angle of 5°. The Reynolds number per foot varied from about 1.6×10^6 to 3.2×10^6.

SYMBOLS

The results of this investigation are presented in coefficient and parameter form, referred to the stability axes for longitudinal data and the body axes for lateral-directional data. The moment reference was at $0.25\bar{c}$ in the chord plane of the wing, and was 16.5 inches forward of the model base.

C_L lift coefficient, $\frac{\text{Lift}}{qS}$

C_D drag coefficient, $\frac{\text{Drag}}{qS}$

C_m pitching-moment coefficient about $0.25\bar{c}$, $\frac{\text{Pitching moment}}{qS\bar{c}}$

C_l rolling-moment coefficient, $\frac{\text{Rolling moment}}{qSb}$

C_n yawing-moment coefficient, $\frac{\text{Yawing moment}}{qSb}$

C_Y side-force coefficient, $\frac{\text{Side force}}{qS}$

C_{L_α} lift-curve slope, $\partial C_L/\partial\alpha$, per deg

$C_{m_{C_L}}$ longitudinal-stability parameter, $\partial C_m/\partial C_L$

$\frac{\partial C_D}{\partial C_L^2}$ drag-due-to-lift factor

C_{l_β} effective-dihedral parameter, $\Delta C_l/\Delta\beta$, per deg

C_{n_β} directional-stability parameter, $\Delta C_n/\Delta\beta$, per deg

C_{Y_β} side-force parameter, $\Delta C_Y/\Delta\beta$, per deg

L/D lift-drag ratio, C_L/C_D

b wing span, in.

[redacted]

c	wing chord, in.
$\bar{c}$	mean aerodynamic chord, based on total wing area, in.
M	free-stream Mach number
q	free-stream dynamic pressure, lb/sq ft
R	Reynolds number per foot
S	wing area, sq ft
$\frac{x_{ac}}{\bar{c}}$	aerodynamic-center location
α	angle of attack, deg
β	angle of sideslip, deg

Subscripts:

b	at model base
o	at zero lift
max	maximum

DESCRIPTION OF MODEL

The model consisted of a wing and body to simulate the first-stage recoverable booster (ref. 2) together with upper stages arranged in parallel as shown in figures 1(a) and 1(b). The first-stage booster was sized to provide an estimated take-off wing loading of 120 lb/sq ft for the largest complete configuration and was identical to the model of reference 2. Dimensions of the expendable rocket boosters conformed approximately to those of several boosters currently being developed. The fuselage of the recoverable booster was a semicylinder 6 diameters long with an ogival nose 7 diameters long. The volume of the fuselage was approximately that required if conventional turbojet or turboramjet propulsion were to be utilized. No powerplant packages or inlets were incorporated into the preliminary configuration. The wing had a delta planform with leading-edge sweep of 70° and a wedge-slab section with constant 2-percent thickness rearward of the 40-percent-chord station. (See fig. 1.) The wing section was unsymmetrical and was mounted with the wedge surface adjacent to the fuselage. The root chord was

identical to the fuselage length, and the mean aerodynamic chord, based on the total planform area, was 22.0 inches.

Several rocket boosters and spacecraft were mounted either on the fuselage side or the wing side of the recoverable booster, as shown in figure 1. Thus, either piggyback or underslung arrangements were simulated. For all tests the base of the rocket booster was coincident with the model base. Two rocket boosters were used, as shown in figure 1(c); one was approximately 5.5 diameters long to simulate a single rocket stage, and the other was approximately 13.3 diameters long to simulate a two-stage rocket booster.

Three types of spacecraft were attached in turn to each of the two rocket boosters - a blunted 40° ballistic nose cone, a rocket with a ratio of body diameter to booster diameter of 0.42, and a 70° delta wing with slab sections and semicircular leading edge mounted on the rocket to form a winged rocket. Details of the spacecraft are given in figure 1(c).

Photographs of the take-off or launch configurations are presented in figure 2 and the principal model dimensions are summarized in table I.

APPARATUS AND TESTS

The tests were made in the Langley 8-foot transonic pressure tunnel at Mach numbers from 0.6 to 1.2 and at angles of attack from -2° to 12°. For one configuration, data were obtained at both 0° and 5° sideslip. The range of Reynolds number per foot is shown in figure 3 to vary from about 1.6×10^6 to 3.2×10^6.

Six-component force and moment data were obtained by means of an internally mounted strain-gage balance. The angles of attack and sideslip were corrected for balance and sting deflections under load. Axial force was corrected to correspond to a base pressure, on the recoverable-booster fuselage and that portion of the wing base intercepted by the fuselage, equal to the free-stream static pressure. The base drag on the rocket booster is included in the data. Transition was fixed by a 0.1-inch band of No. 80 carborundum (0.008-inch-diameter grains) at the 5-percent station on all surfaces.

The accuracy of the data has been estimated on the basis of repeatability of data and balance accuracy to be approximately as follows:

M	±0.005
α, deg	±0.1
β, deg	±0.1
C_L	±0.005
C_D	±0.001
C_m	±0.002
C_l	±0.001
C_n	±0.001
C_Y	±0.002

PRESENTATION OF RESULTS

The data fall into three principal divisions: characteristics of configurations with the high-wing recoverable booster, characteristics of configurations with the low-wing recoverable booster, and effects of adding upper stages to the recoverable booster. The data are presented as follows:

DISCUSSION

High-Wing Recoverable Booster

Longitudinal stability.- Comparison of the data of figures 4 and 5 for the high-wing recoverable booster shows that the effects of changing from a one-stage rocket booster to a two-stage rocket booster were generally small. The principal effect was that a small positive increment in $C_{m,o}$ resulted. With the two-stage rocket booster, the spacecraft was forward of the wing leading edge regardless of which spacecraft was installed, and an effective upwash on the wing, coupled with the increased projected area forward of the wing leading edge, caused the stability changes shown. Figure 7 shows that when the spacecraft was located behind the leading edge of the wing, as with the one-stage rocket booster, the only change in longitudinal stability resulting from changing from the ballistic to the winged-rocket spacecraft was a small decrease in stability near $M = 1.0$. However, with the two-stage rocket booster (fig. 8), in which case the spacecraft was forward of the wing leading edge, substitution of the winged-rocket spacecraft for either the ballistic or the rocket spacecraft caused a destabilizing increment in $C_{m_{C_L}}$ of about 0.02 over the Mach number range. This is in good agreement with the value of 0.03 which had been estimated on the basis of the centroid of the combined areas of the first-stage wing and spacecraft wing. Comparison of figures 7 and 8 for the configurations with the winged-rocket spacecraft shows that a decrease in static margin occurred when the two-stage rocket booster was used (winged-rocket spacecraft in front of leading edge of recoverable-booster wing) rather than the one-stage rocket booster (winged-rocket spacecraft behind leading edge of recoverable-booster wing). Furthermore, it is seen that the increase in static margin with M was more abrupt for the arrangements with the one-stage rocket booster than for those with the two-stage rocket booster.

Figures 6 and 9 show that the principal effect of moving the two-stage rocket booster and winged-rocket spacecraft from the wing side (piggyback) to the fuselage side (underslung) of the high-wing recoverable booster was a small decrease in the longitudinal stability which varied from about 0.010 to 0.015 over the Mach number range. As previously mentioned, when the spacecraft was situated behind the leading edge of the wing of the recoverable booster, only small changes in stability occurred when the winged-rocket spacecraft was installed; therefore, it is believed that with the one-stage rocket booster the change in position from piggyback to underslung would cause less change in stability than shown in figure 9. Thus it is concluded that the measured changes in longitudinal stability due to the position of the upper stages should not be detrimental to the choice of either arrangement.

The effects of the several upper-stage arrangements are shown in figure 10 in terms of the aerodynamic-center location. In this figure the shift in aerodynamic-center location with Mach number for the one-stage rocket booster and spacecraft is nearly 15 percent, whereas that for the two-stage rocket booster and spacecraft is only about 9 percent. Generally the spacecraft configuration and the change from a piggyback to an underslung arrangement did not affect the aerodynamic-center shift in the transonic speed range.

Drag and L/D.- The data from which the zero-lift drag-coefficient curves of figures 7, 8, and 9 were derived have been supplemented by the addition of test points at $M = 0.94$ and 1.02. Comparison of figures 7 and 8 shows that when the one-stage rocket booster was used the drag rise near sonic speed was larger and steeper than when the two-stage rocket booster was used. Such a result would be expected from the more adverse area distribution of the configuration with the one-stage rocket booster. The entire booster frontal area of the one-stage rocket booster must be added near the peak of the area-distribution curve for the recoverable booster alone. Figure 9 indicates that, from a drag standpoint, neither the piggyback nor the underslung arrangement is to be preferred.

Figure 11 shows that the installation of the winged-rocket spacecraft generally resulted in a small decrease in maximum L/D and that this decrease was greatest when the two-stage rocket booster was used. Also shown is the fact that mounting the upper stages on the fuselage side (underslung) gave slightly higher values of $(L/D)_{max}$ than mounting them on the wing side (piggyback), although the differences were small. This characteristic probably will not continue into the hypersonic speed range.

Low-Wing Recoverable Booster

Longitudinal stability.- As previously observed for the high-wing recoverable-booster arrangements, figures 12 and 13 show that with the low-wing recoverable booster the effects of interchanging the one- and two-stage rocket boosters and of interchanging the spacecraft were small. A small negative change in $C_{m,o}$ resulted from installation of the two-stage rocket booster in place of the single-stage rocket booster. When the winged-rocket spacecraft was attached to either the one- or two-stage rocket booster a small destabilizing increment in $C_{m_{C_L}}$, as shown in figures 15 and 16, was experienced. This increment was about 0.01 for the one-stage rocket booster and about 0.02 for the two-stage rocket booster and was approximately uniform throughout the Mach number range. Mounting the winged-rocket spacecraft and two-stage rocket booster on the fuselage side (piggyback) rather than in the underslung position caused a decrease in static margin varying from 1.5 to 3 percent. (See figs. 14 and 17.) This result is similar to that observed for the high-wing configuration. Figure 18 shows that the aerodynamic-center shift with Mach number was again greater for the configuration with one-stage rocket booster and spacecraft than for the configuration with two-stage rocket booster and spacecraft. The aerodynamic-center shift for the former was about 10 percent, whereas the shift for the latter was only 8 percent. In all cases, the aerodynamic-center shift was essentially independent of the spacecraft configuration or the position of the upper stages (piggyback or underslung).

Drag and L/D.- Figures 15 and 16 show that the transonic drag rise for the low-wing arrangement was essentially independent of the spacecraft, but as mentioned earlier for the high-wing arrangement, the one-stage rocket booster produced larger transonic drag rise than the two-stage rocket booster, and the drag rise commenced at a lower Mach number and was more abrupt, as well. Furthermore, figure 17 shows that the position of the upper stages had no effect on the transonic drag-rise characteristics. Figure 19 shows that small decreases in maximum L/D resulted when the winged-rocket spacecraft was installed on the rocket boosters. Insignificant differences in maximum L/D are shown for the two rocket boosters, the three spacecraft, and the two upper-stage positions (piggyback and underslung).

Recoverable Booster Without and With Upper Stages

Data from reference 2, which reports the characteristics of the recoverable booster, have been compared with the results of the present tests to ascertain the aerodynamic effects of adding large upper stages. The configuration selected for the comparison consisted of the low-wing recoverable booster with the two-stage rocket booster and winged-rocket spacecraft mounted in the underslung position. These upper stages were

selected because they were the largest ones tested and would be expected to produce the largest changes.

The effect of the upper stages on the longitudinal stability is shown in figure 20 for the selected moment reference. The stability change is shown to be negligible. Examination of the curves from which figure 20 was derived showed that a negligible change in $C_{m,o}$ resulted when these upper stages were added. Changes in the flow field near the leading edge of the first-stage wing, caused by the location of the spacecraft forward of the wing, apparently compensated for the moment contribution due to the drag of the rocket booster to result in this small change in $C_{m,o}$. The drag-coefficient change shown in figure 20, however, is significant. At subsonic speeds, the drag-coefficient increase was about 0.004, of which the base drag of the rocket booster contributed about 0.0015 and the increase in skin friction contributed an estimated 0.002. At $M = 1.2$ the increment increased to about 0.008, which amounts to about a 50-percent increase over the drag coefficient of the recoverable booster alone. This drag increase could have been substantially reduced by the addition of a closure fairing on the base of the rocket booster, since the drag coefficients shown include the base drag of this booster, which is estimated to be about 0.003 at $M = 1.2$. The transonic drag level will probably be a major controlling factor in the design of a suitable powerplant configuration for the recoverable booster, inasmuch as it is desirable to have a large excess of thrust over drag to reduce the acceleration fuel required.

The aerodynamic characteristics at a sideslip angle of 5° are shown for the recoverable booster without and with the upper stages in figure 21, and the lateral-directional stability derivatives are shown in figure 22. Installing the upper stages caused little change in the magnitude of the effective-dihedral parameter C_{l_β} but decreased the directional stability as much as 50 percent. The large increase in the side-force parameter also demonstrates the effect of the large upper stages. Because of the great reduction in C_{n_β} coupled with the high values of C_{l_β} at high angle of attack, configurations such as this may encounter Dutch roll oscillations at the steep climb attitude expected for this type of vehicle. This tendency may be alleviated by an increase in the effective vertical-fin area to increase the directional stability, an improvement believed necessary for hypersonic speeds.

SUMMARY OF RESULTS

An investigation at transonic speeds has been made in the Langley transonic pressure tunnel to ascertain the aerodynamic characteristics

of several launch configurations composed of large expendable rocket boosters and various spacecraft mounted in parallel with one concept of a horizontal-take-off-and-horizontal-landing recoverable booster. The data have been compared with previously obtained data for the recoverable booster alone to determine the effects of the addition of the upper stages to the recoverable booster. The principal results were as follows:

1. The changes in longitudinal stability caused by using a two-stage rocket booster rather than a one-stage rocket booster were small. Neither a piggyback nor an underslung arrangement seemed to offer particular advantages.

2. For all upper-stage arrangements, the winged-rocket spacecraft produced a small reduction in static margin which was less when the spacecraft wing was located behind the leading edge of the first-stage wing than ahead of it.

3. Arrangements with the one-stage rocket booster resulted in higher transonic drag than those with the two-stage rocket booster.

4. Neither the high-wing nor the low-wing arrangements demonstrated superior transonic-drag or drag-rise characteristics.

5. Addition of the largest upper stages did not change the longitudinal stability of the basic recoverable booster.

6. Addition of the upper stages caused a transonic drag increase of about 50 percent of the value for the recoverable booster alone, but a sizable reduction could be achieved by addition of suitable closure fairings at the rocket base.

7. Addition of the upper stages did not change the lateral stability, but reduced the directional stability nearly 50 percent.

Langley Research Center,
National Aeronautics and Space Administration,
Langley Station, Hampton, Va., May 1, 1962.

REFERENCES

1. Pierpont, P. Kenneth: Transonic Stability of a Preliminary Vertical-Take-Off Launch Configuration With a Horizontal-Landing Recoverable Booster. NASA TM X-689, 1962.

2. Pierpont, P. Kenneth: Transonic Longitudinal and Lateral Aerodynamic Characteristics of a Preliminary Concept of a First-Stage Horizontal-Take-Off-and-Horizontal-Landing Recoverable Booster With a 70° Delta Wing. NASA TM X-691, 1962.

TABLE I.- GEOMETRIC CHARACTERISTICS OF MODEL

Recoverable booster:	
Fuselage:	
Length, in.	33.00
Diameter, in.	2.52
Forebody fineness ratio	7.0
Afterbody fineness ratio	6.1
Base area, sq in.	4.16
Wing:	
Total area, sq in.	396
Span, in.	24.00
Root chord, in.	33.00
Tip chord, in.	0
Thickness, percent chord	2
Leading-edge sweep angle, deg	70.0
Mean aerodynamic chord, in.	22.00
Moment reference center, percent $\bar{c}$	25
Moment reference center, in. from base	16.5
Vertical tail:	
Area (exposed), sq in.	16.43
Span (exposed), in.	3.46
Root chord, in.	9.50
Tip chord, in.	0
Thickness, percent chord	2
Leading-edge sweep angle, deg	70.0
One-stage rocket booster:	
Length, not including interstage, in.	13.08
Diameter, in.	2.40
Length/Diameter	5.5
Two-stage rocket booster:	
Length, not including interstage, in.	31.92
Diameter, in.	2.40
Length/Diameter	13.3
Ballistic spacecraft:	
Length, in.	2.33
Base diameter, in.	2.40
Nose-cone included angle, deg	40.0
Nose radius, in.	0.50
Rocket spacecraft:	
Length, including interstage, in.	8.04
Diameter, in.	1.00
Nose-cone included angle, deg	40.0
Nose radius, in.	0.20
Winged-rocket spacecraft:	
Body diameter, in.	1.00
Length, including interstage, in.	8.04
Nose-cone included angle, deg	40.0
Nose radius, in.	0.20
Wing area, total, sq in.	15.38
Wing area, exposed, sq in.	9.69
Wing thickness, percent chord	10
Leading-edge radius, percent chord	5
Root chord, in.	6.5
Tip chord, in.	0
Leading-edge sweep angle, deg	70.0

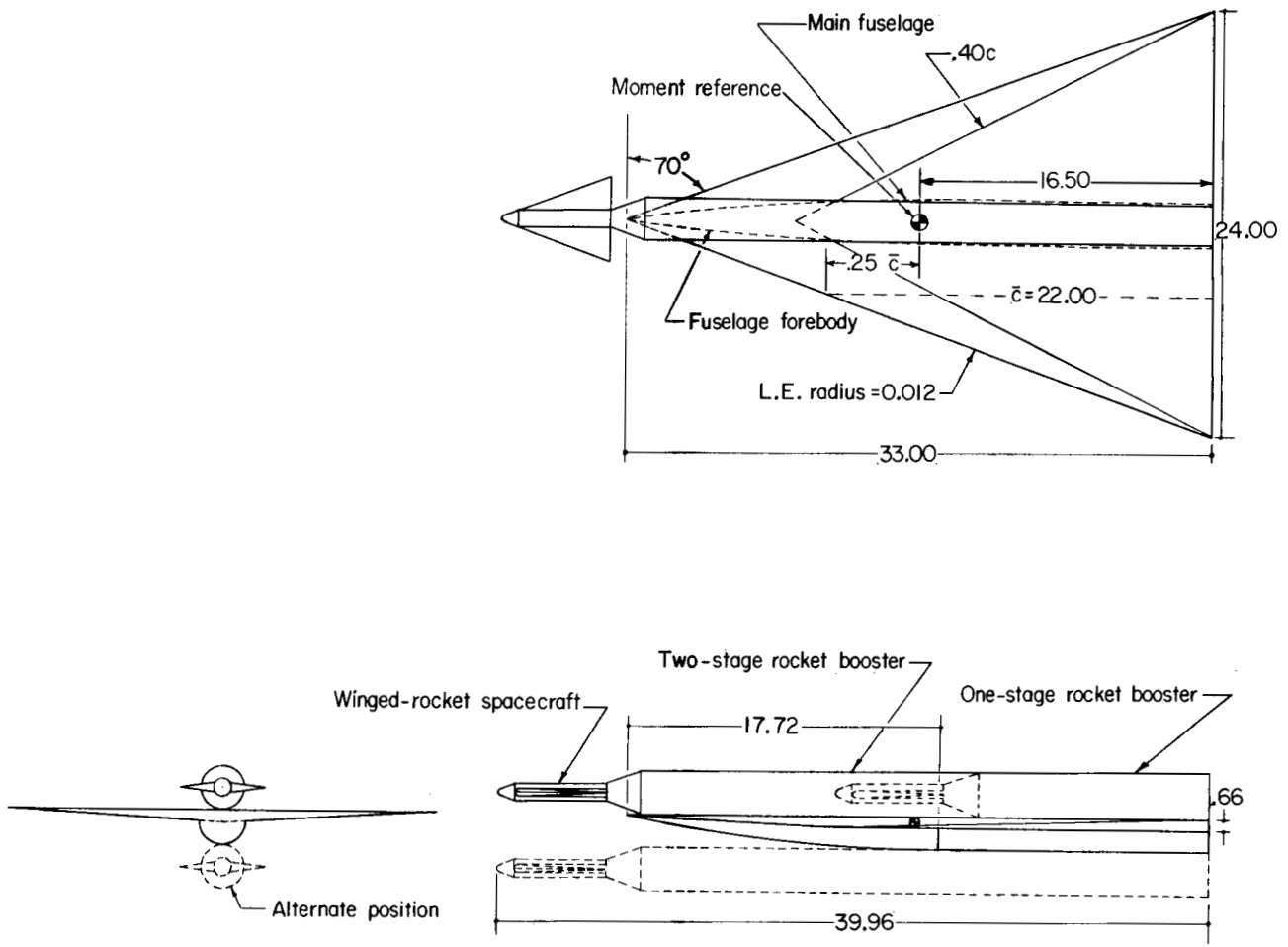

(a) High-wing arrangement (flat-top wing).

Figure 1.- Horizontal-take-off-and-horizontal-landing recoverable booster and upper stages. All linear dimensions are in inches.

UNCLASSIFIED

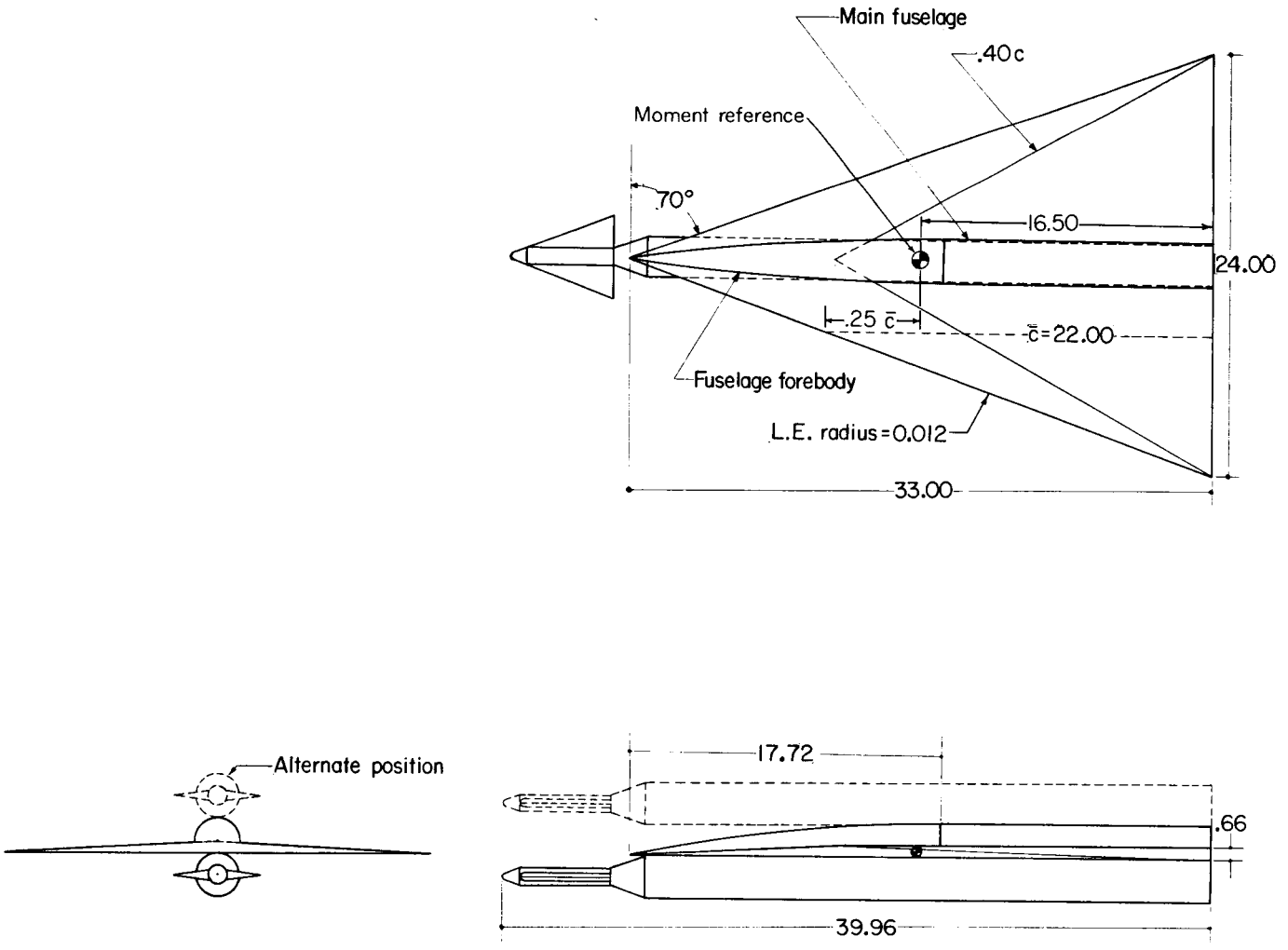

(b) Low-wing arrangement (flat-bottom wing).

Figure 1.- Continued.

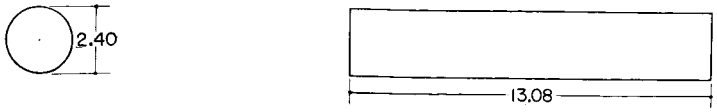

One-stage rocket booster

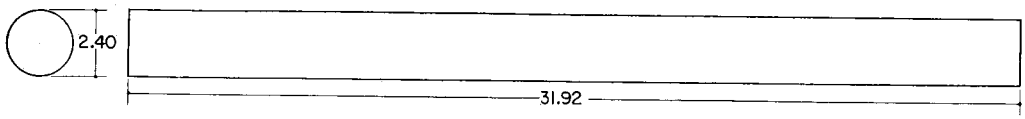

Two-stage rocket booster

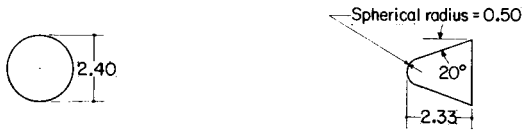

Ballistic spacecraft

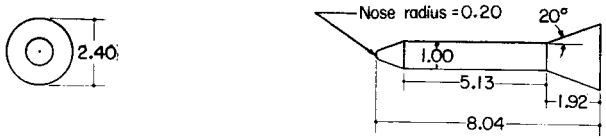

Rocket spacecraft

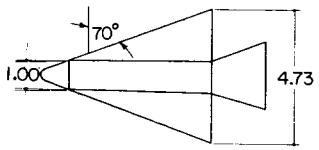

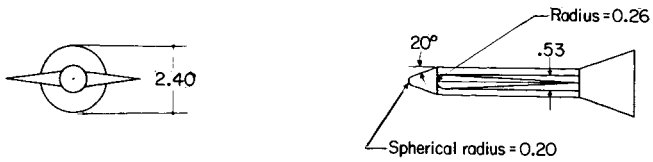

Winged-rocket spacecraft

(c) Dimensions of rocket boosters and spacecraft.

Figure 1.- Concluded.

L-1935

[redacted]

UNCLASSIFIED

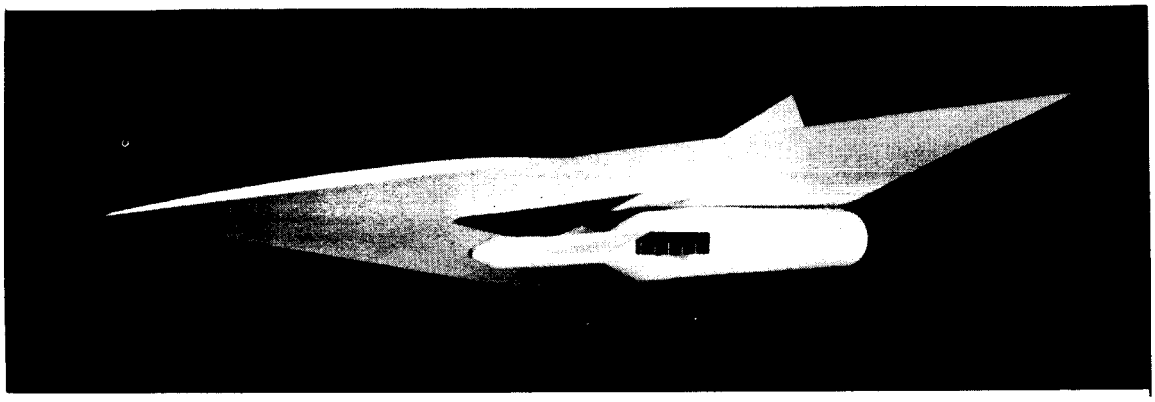

(a) Winged-rocket spacecraft attached to one-stage rocket booster mounted beneath low-wing recoverable booster.

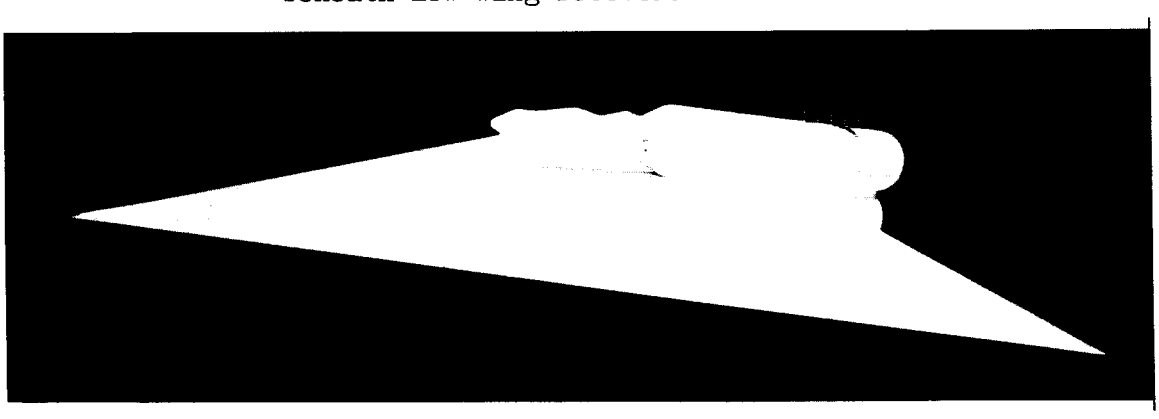

(b) Winged-rocket spacecraft attached to one-stage rocket booster mounted on top of low-wing recoverable booster.

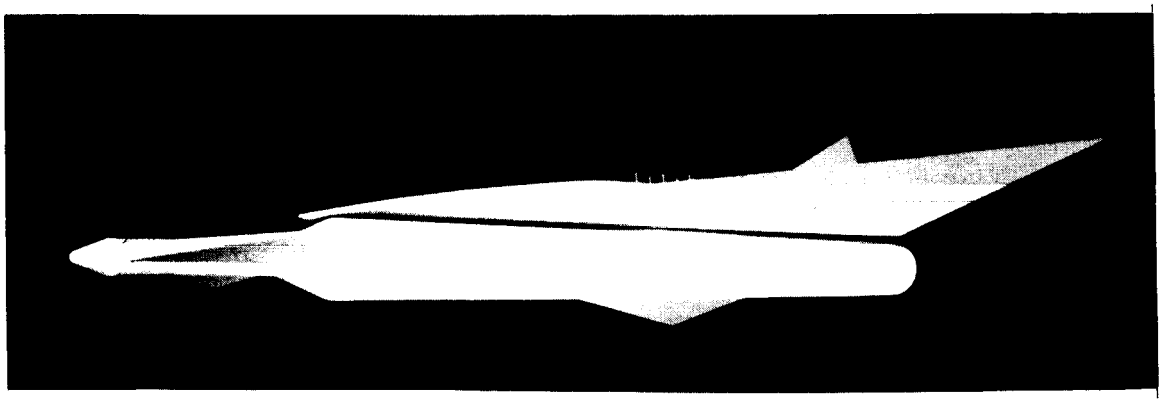

(c) Winged-rocket spacecraft attached to two-stage rocket booster mounted beneath low-wing recoverable booster.

L-62-2052

Figure 2.- Photographs of HTOHL recoverable booster with various upper-stage arrangements.

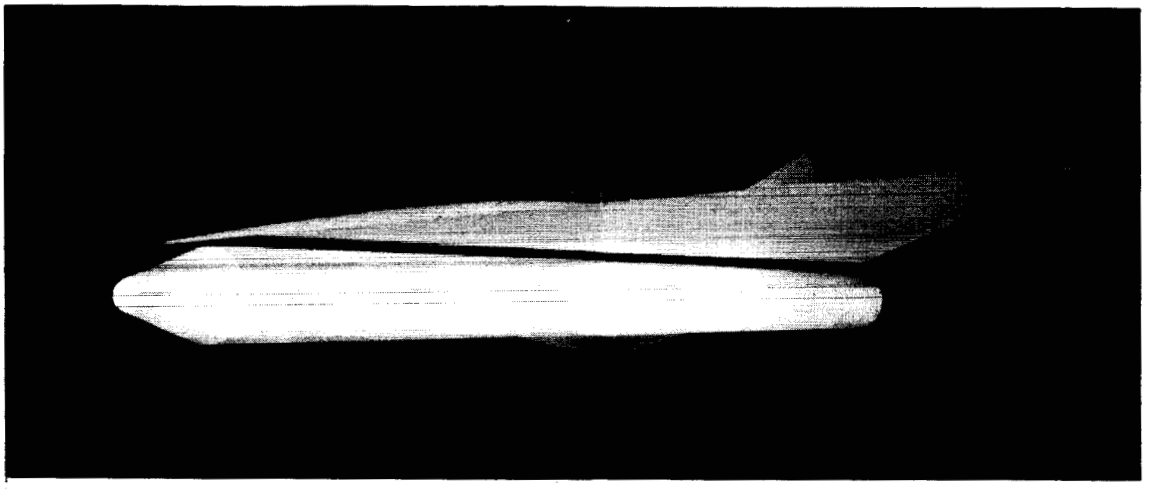

(d) Ballistic spacecraft attached to two-stage rocket booster mounted beneath low-wing recoverable booster.

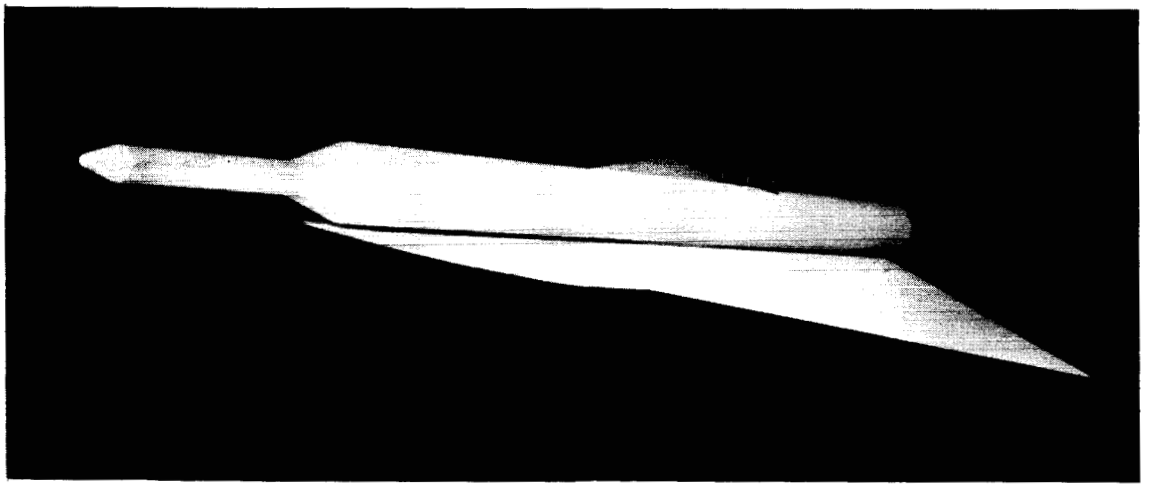

L-62-2053

(e) Ballistic spacecraft attached to two-stage rocket booster mounted on top of high-wing recoverable booster.

Figure 2.- Concluded.

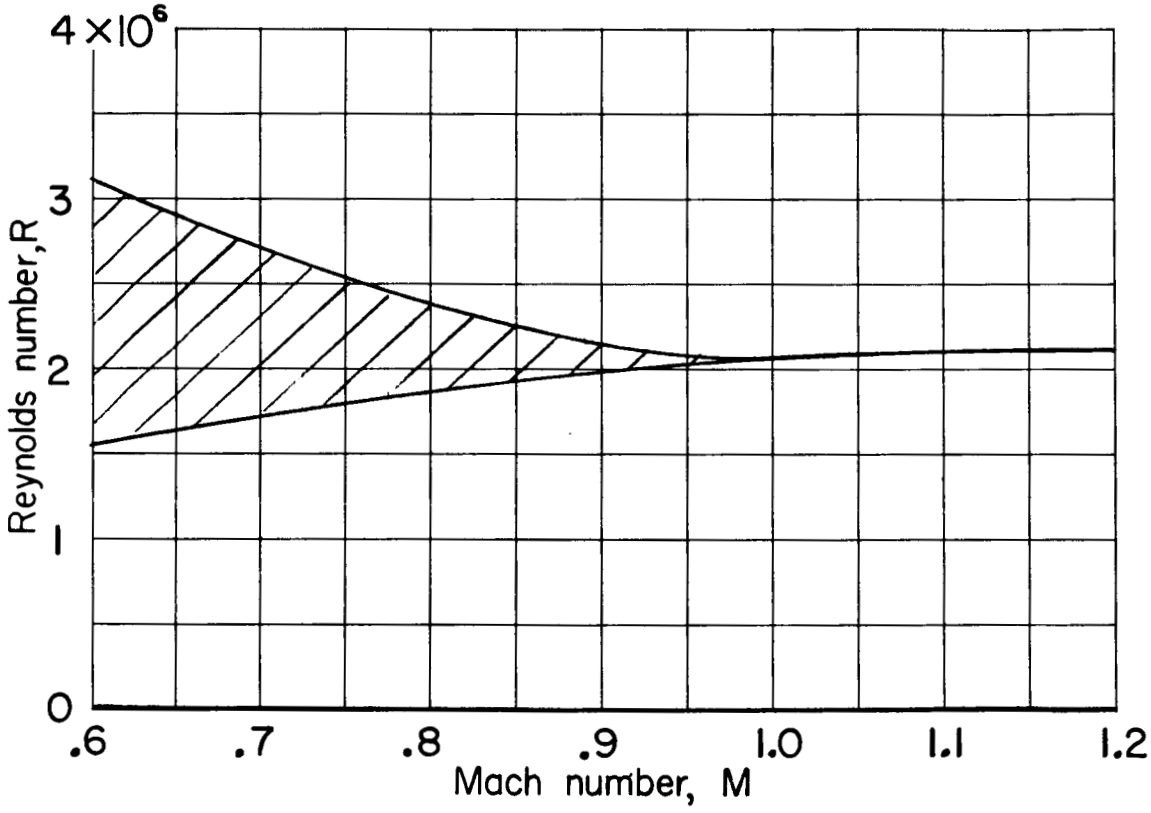

Figure 3.- Variation with Mach number of test Reynolds number per foot.

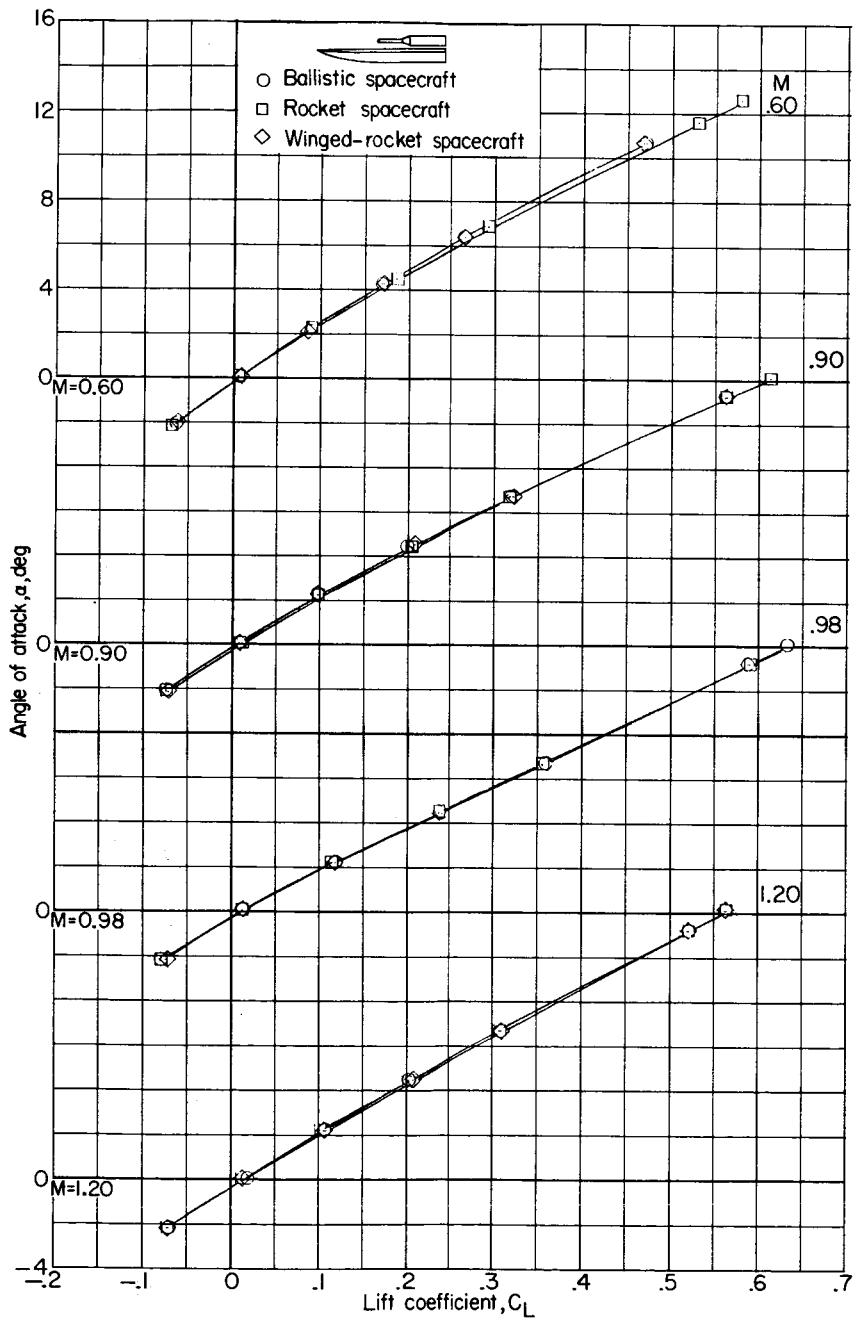

(a) Variation of lift coefficient with angle of attack.

Figure 4.- Aerodynamic characteristics of the several spacecraft attached to a one-stage rocket booster mounted on top of the high-wing recoverable booster.

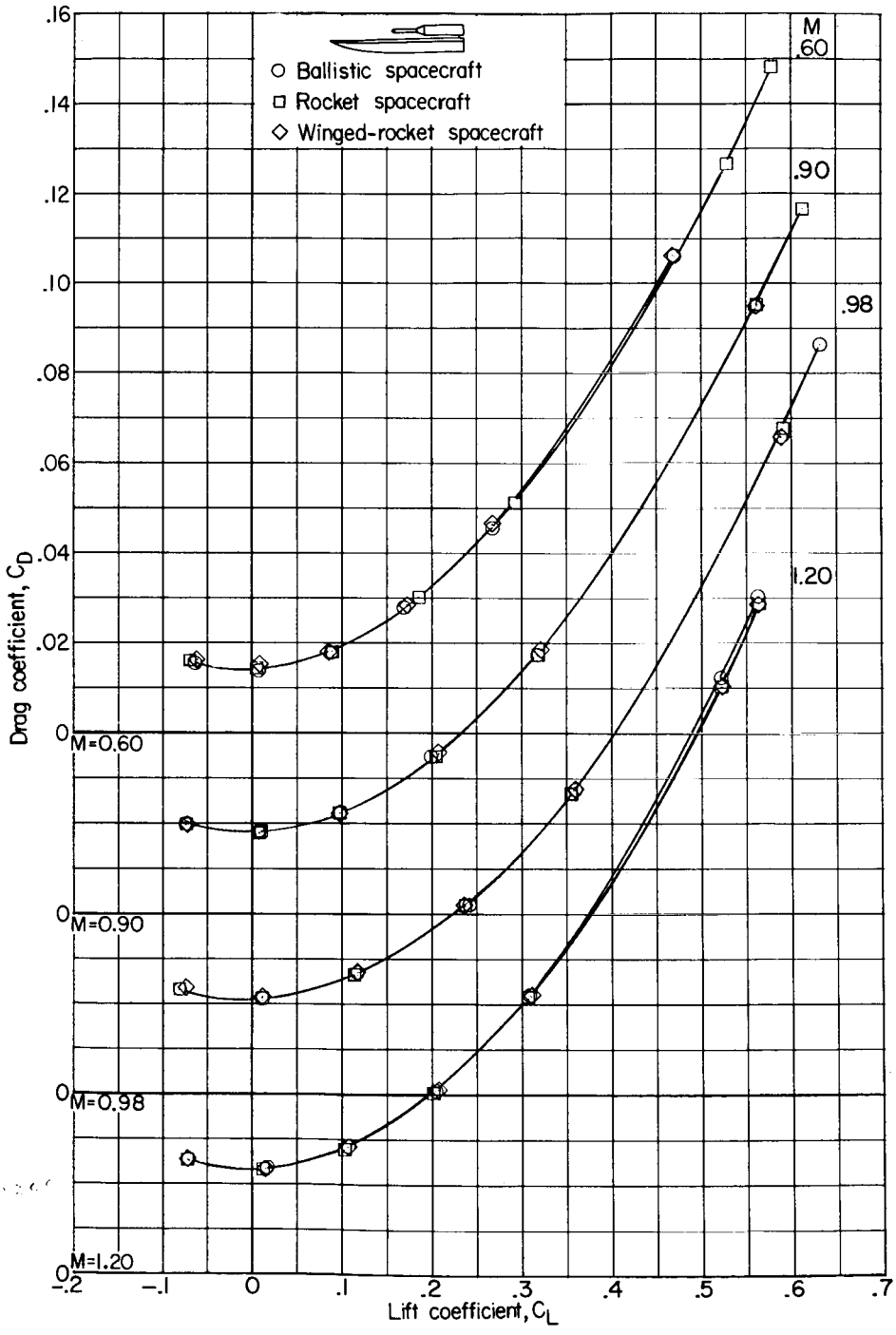

(b) Variation of drag coefficient with lift coefficient.

Figure 4.- Continued.

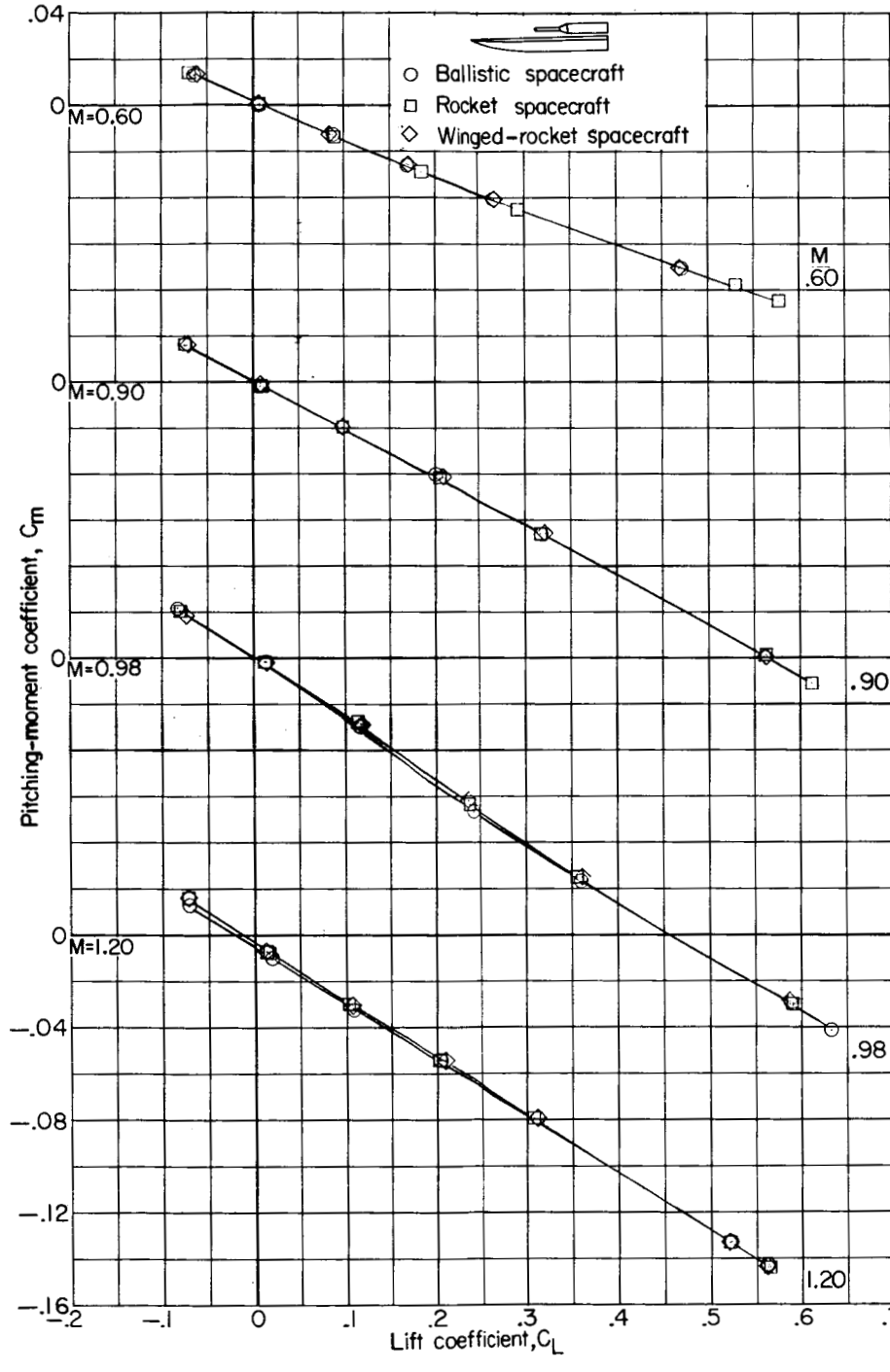

(c) Variation of pitching-moment coefficient with lift coefficient.

Figure 4.- Continued.

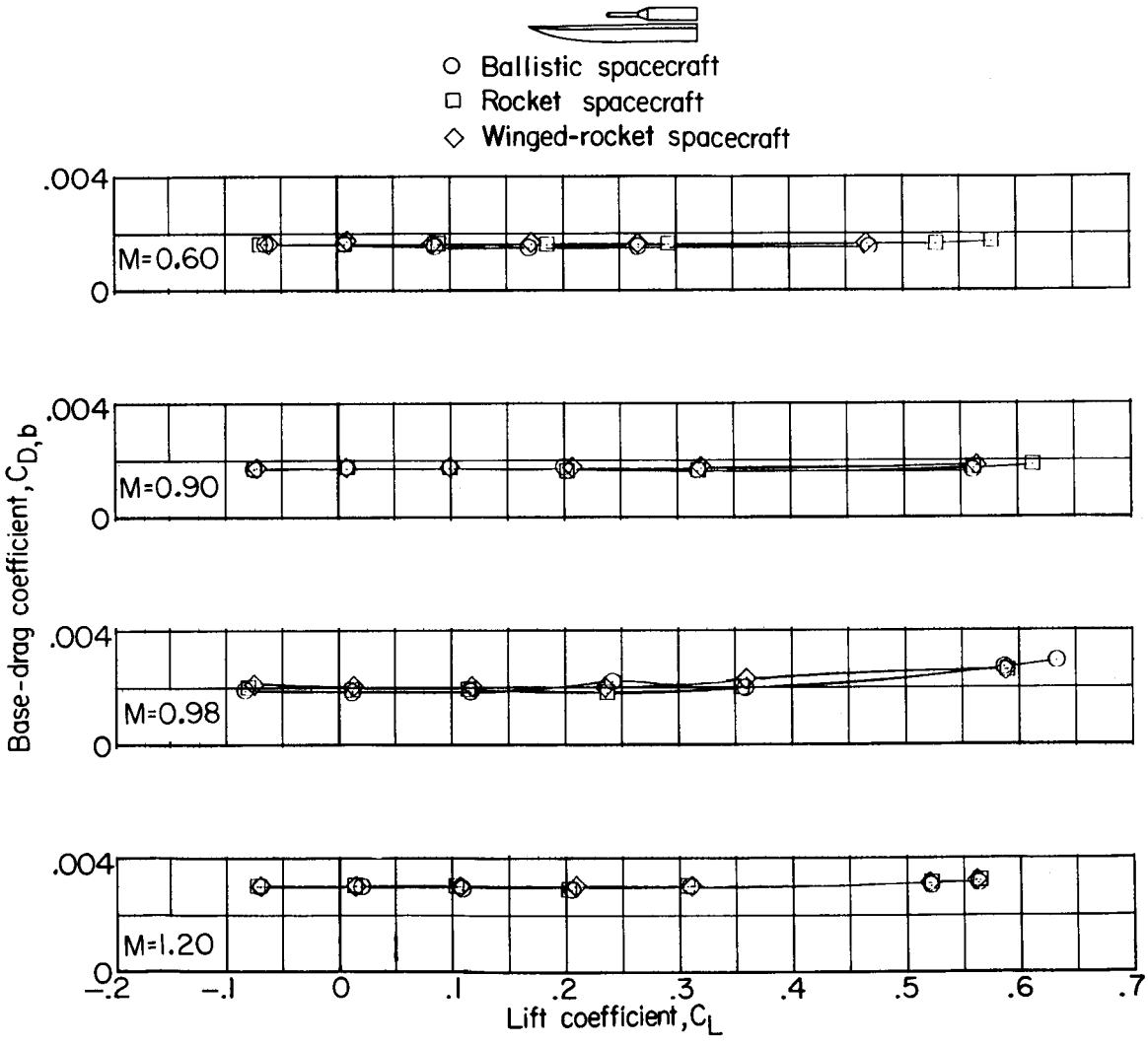

(d) Variation of base-drag coefficient with lift coefficient.

Figure 4.- Concluded.

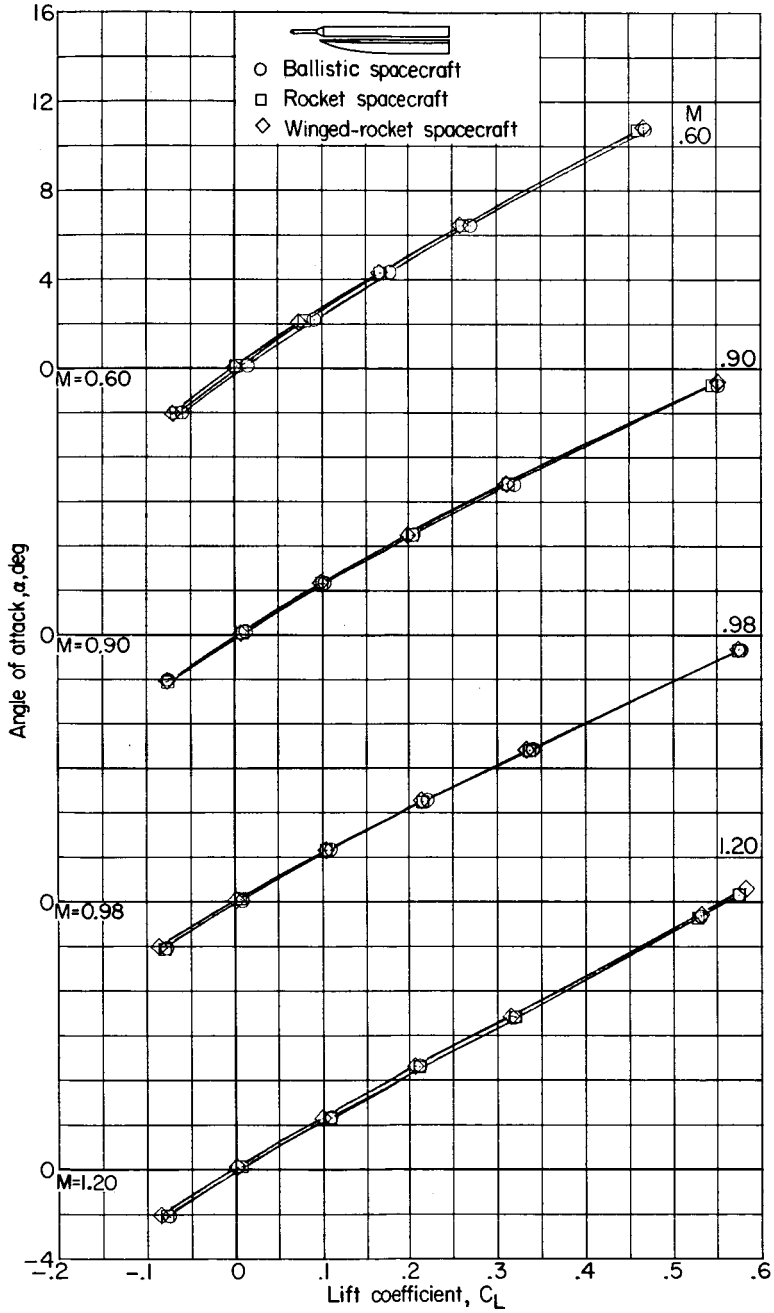

(a) Variation of lift coefficient with angle of attack.

Figure 5.- Aerodynamic characteristics of the several spacecraft attached to a two-stage rocket booster mounted on top of the high-wing recoverable booster.

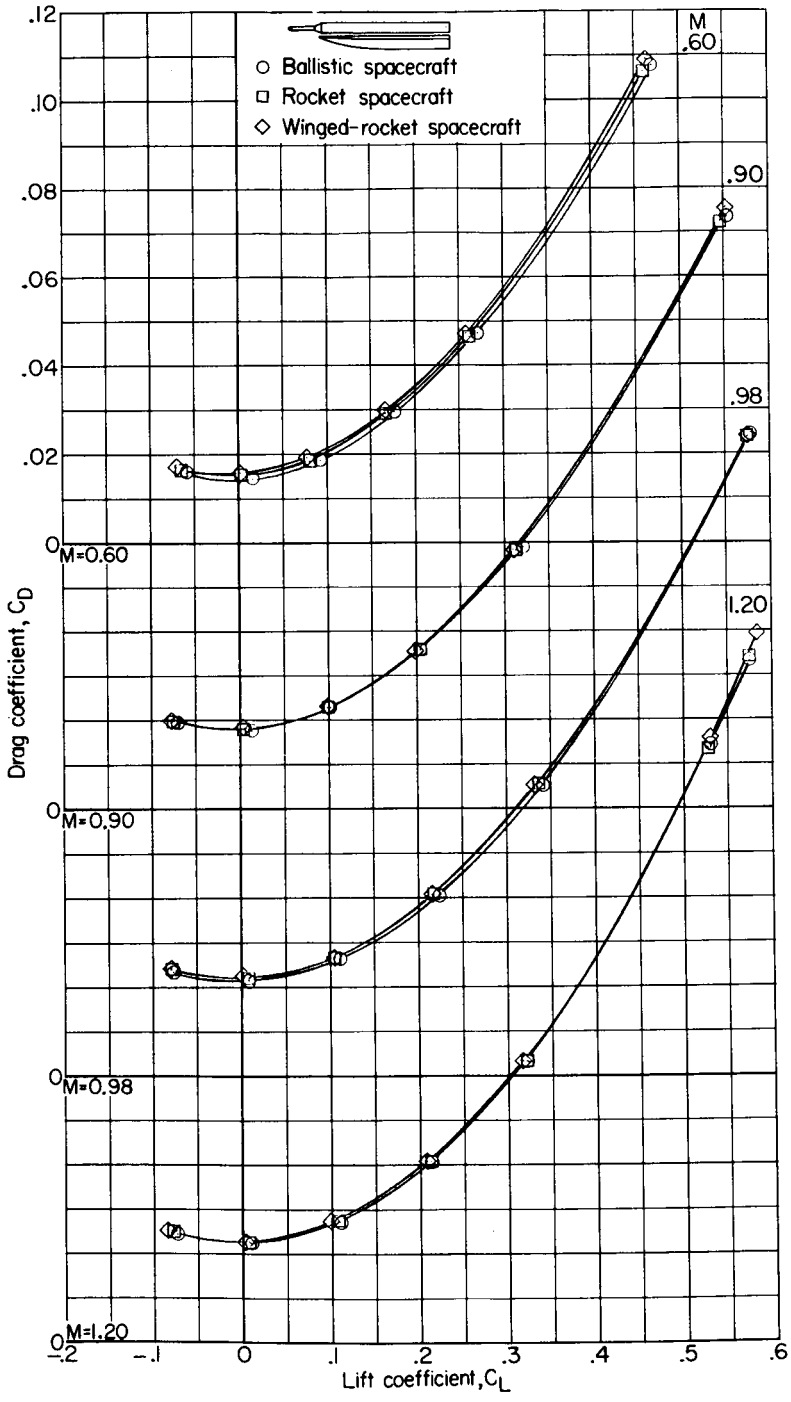

(b) Variation of drag coefficient with lift coefficient.

Figure 5.- Continued.

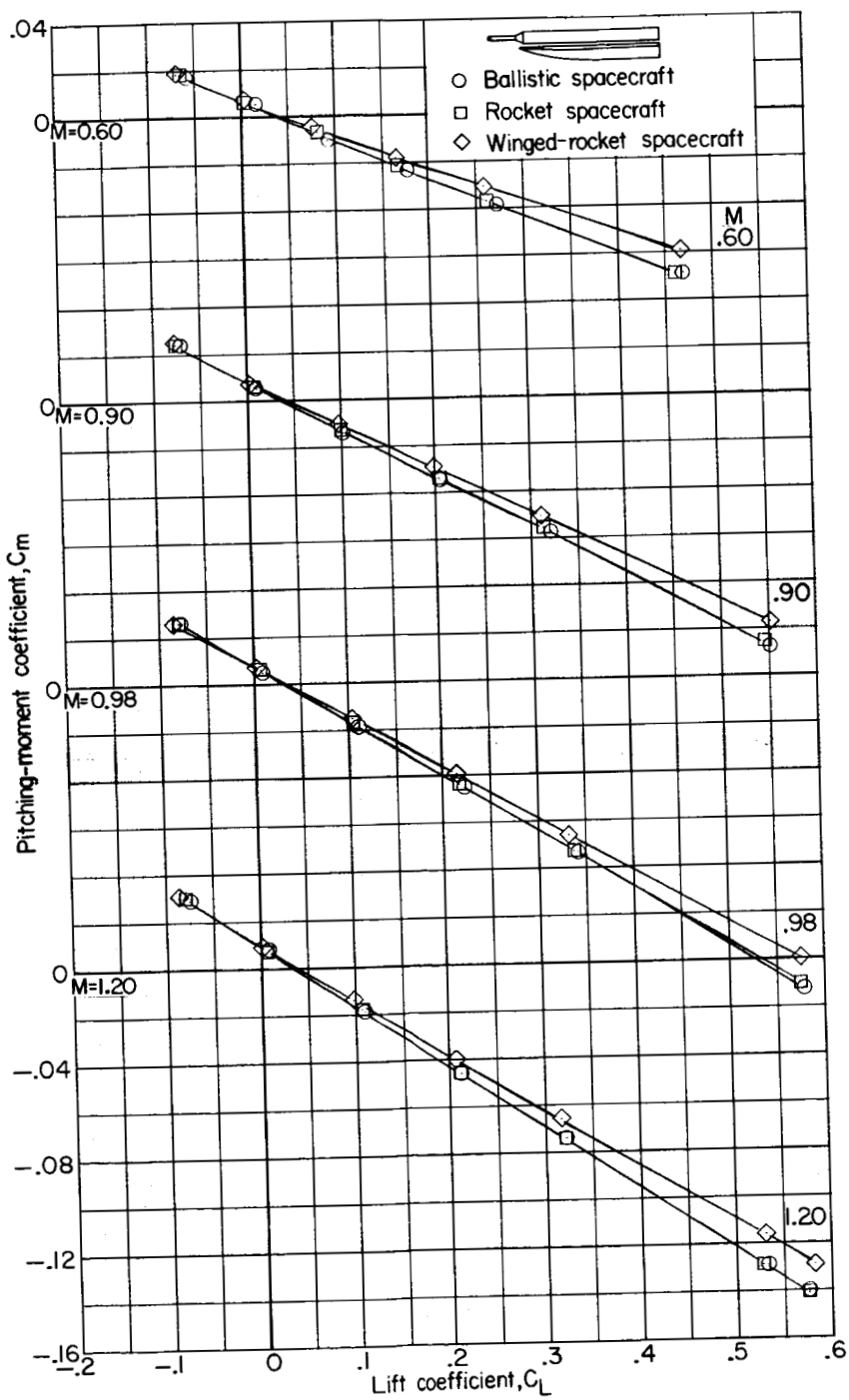

(c) Variation of pitching-moment coefficient with lift coefficient.

Figure 5.- Continued.

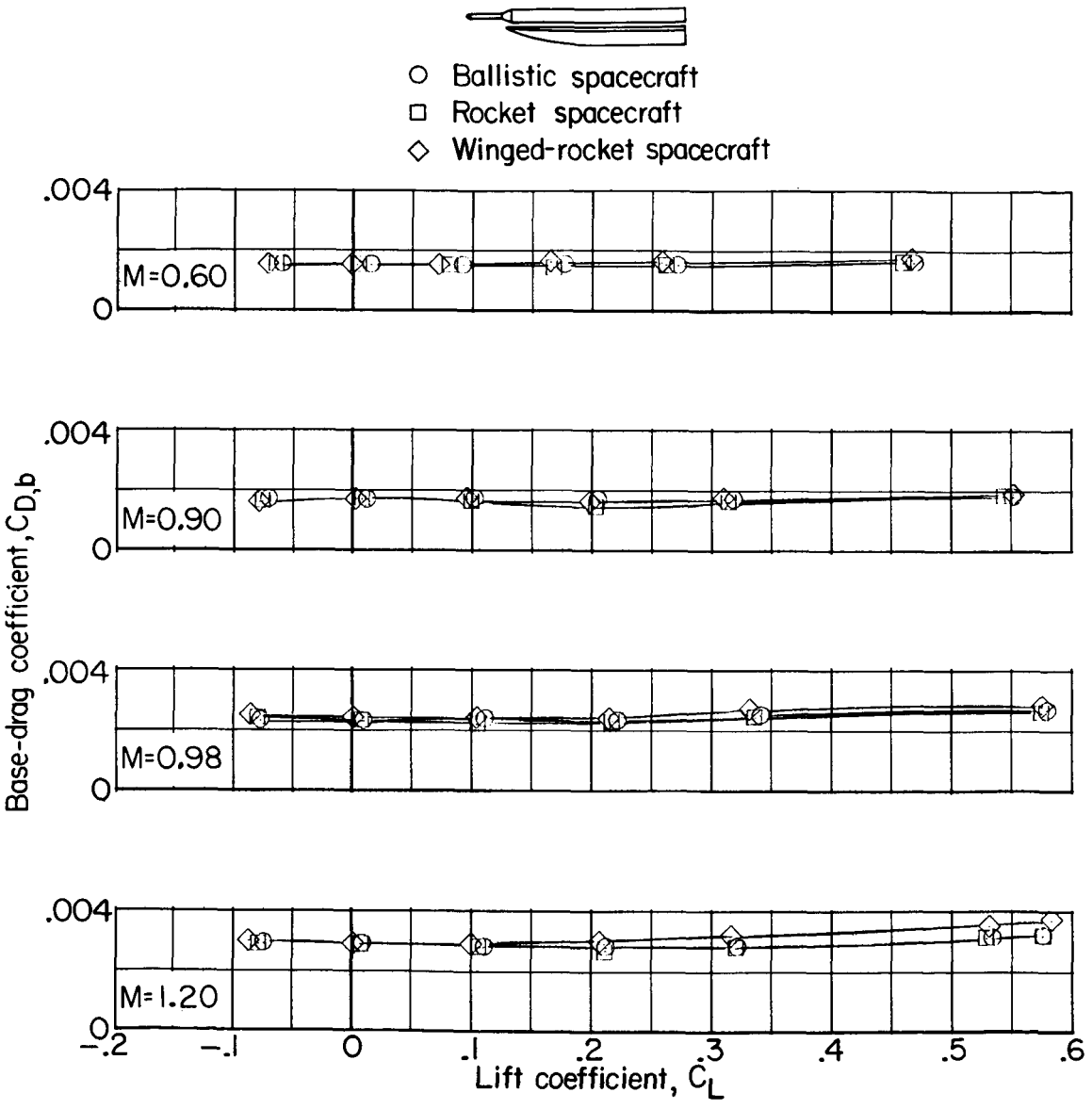

(d) Variation of base-drag coefficient with lift coefficient.

Figure 5.- Concluded.

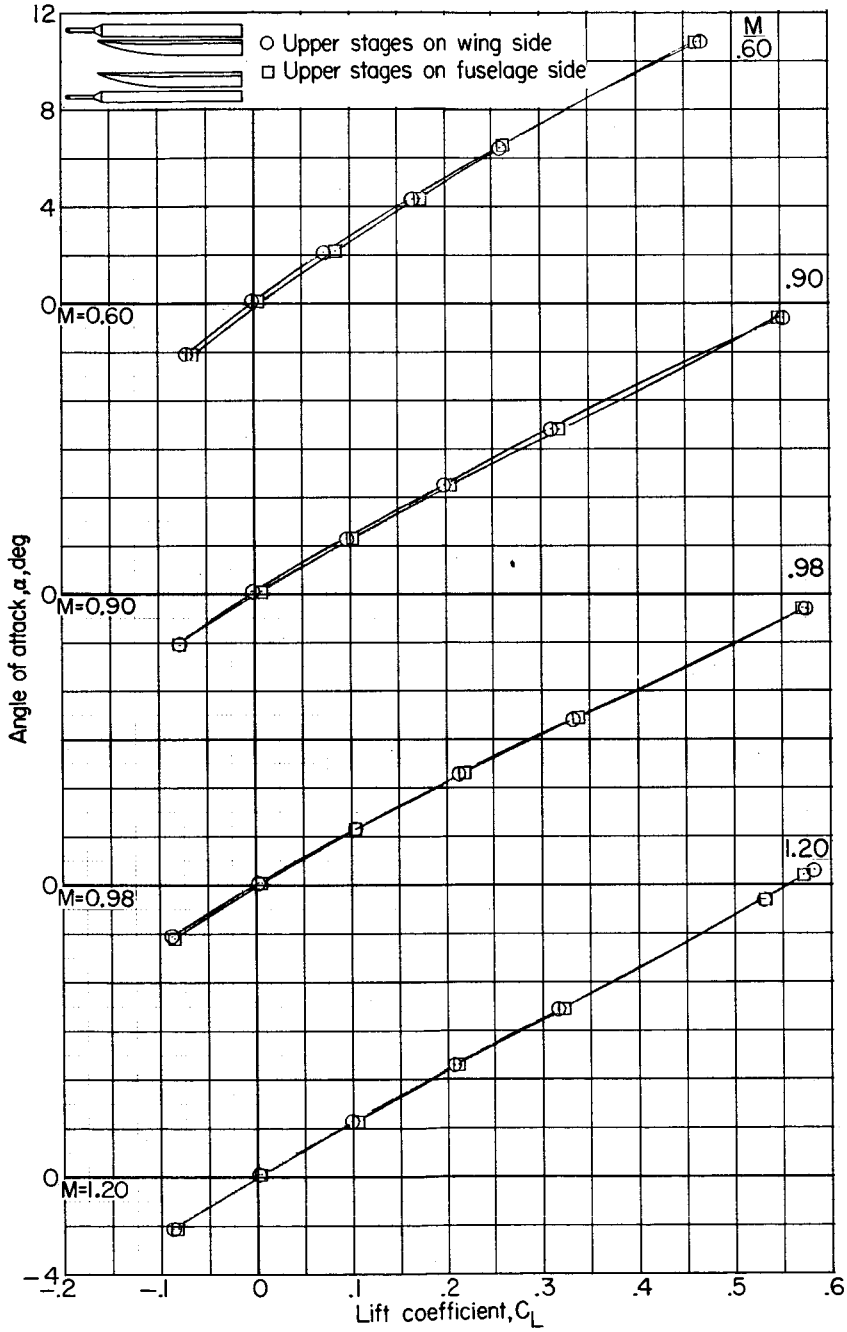

(a) Variation of lift coefficient with angle of attack.

Figure 6.- Aerodynamic characteristics of the winged-rocket spacecraft attached to a two-stage rocket booster mounted above or beneath the high-wing recoverable booster.

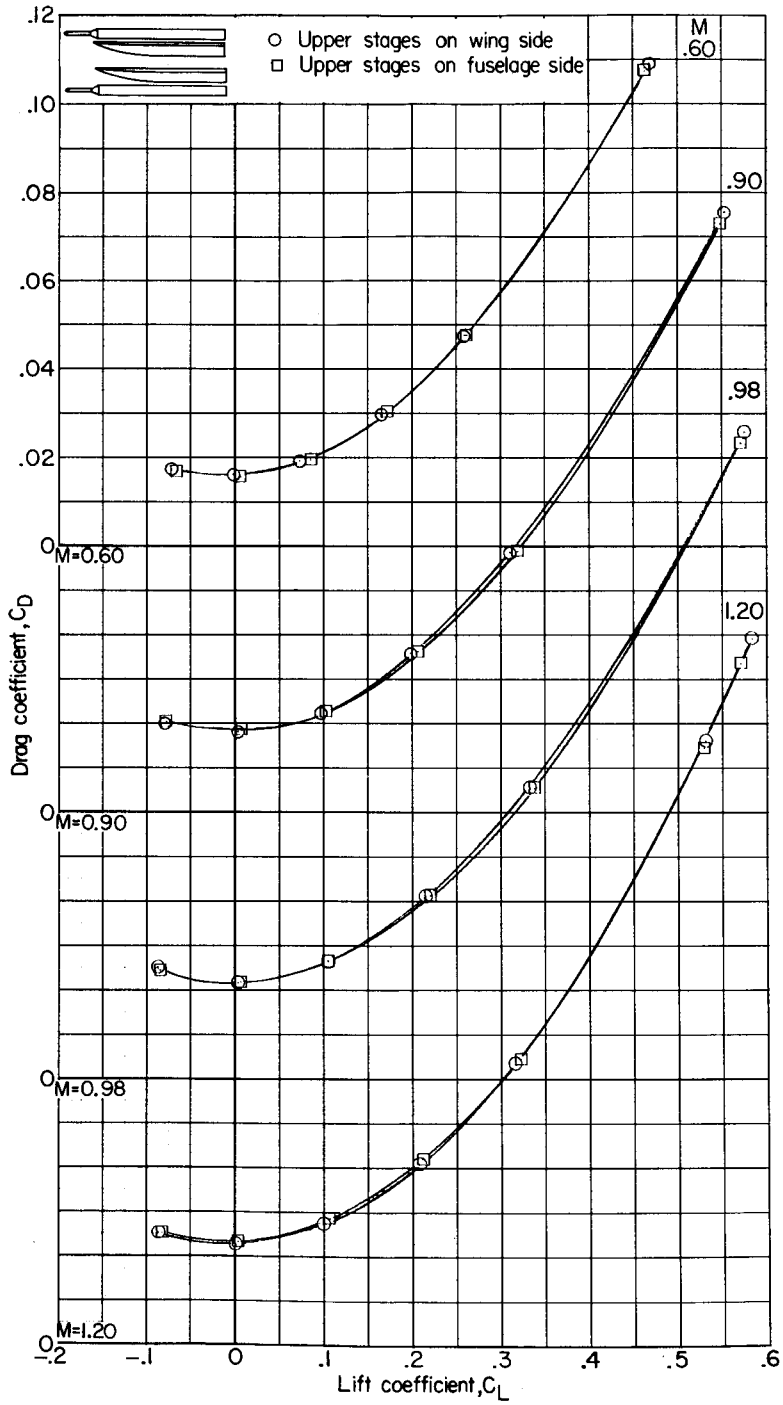

(b) Variation of drag coefficient with lift coefficient.

Figure 6.- Continued.

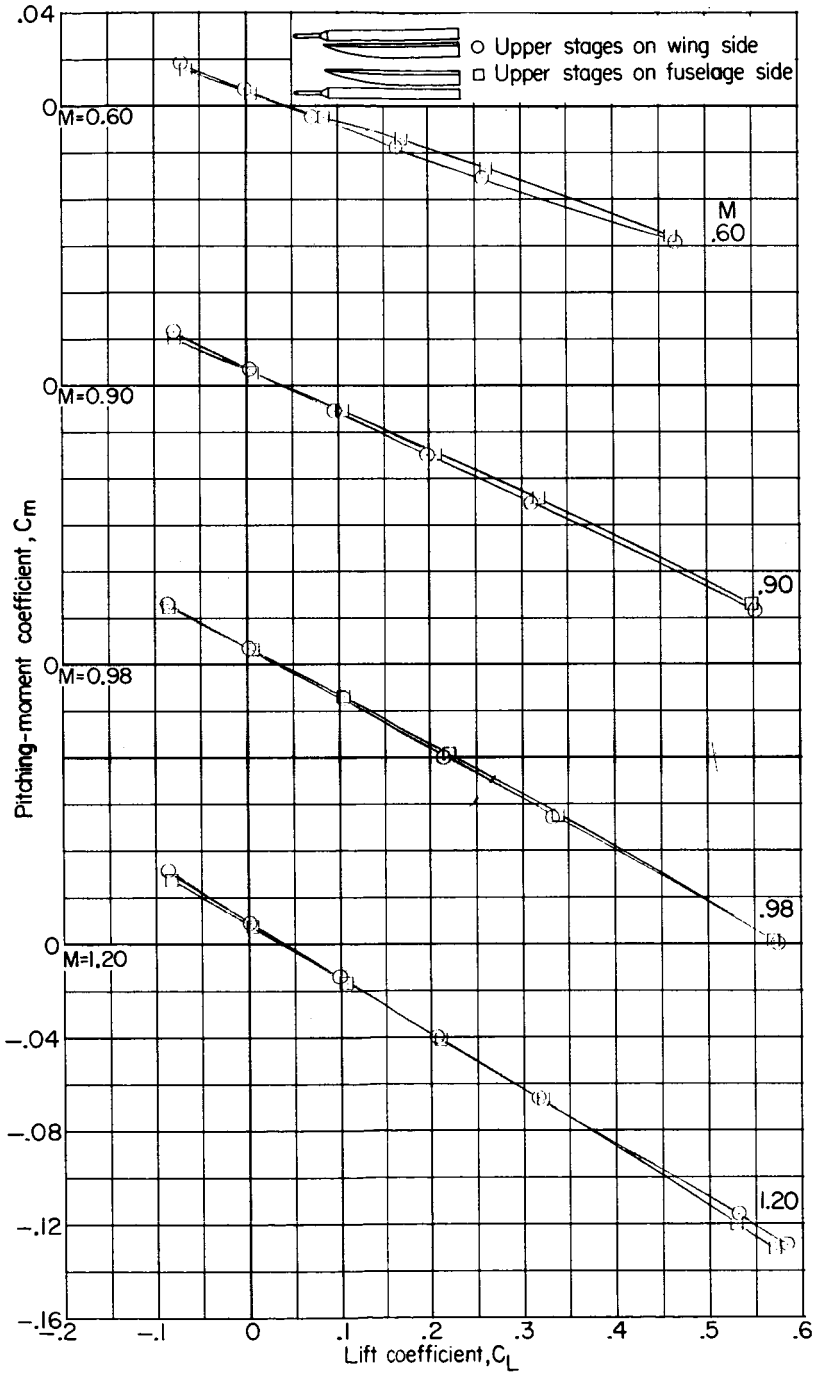

(c) Variation of pitching-moment coefficient with lift coefficient.

Figure 6.- Continued.

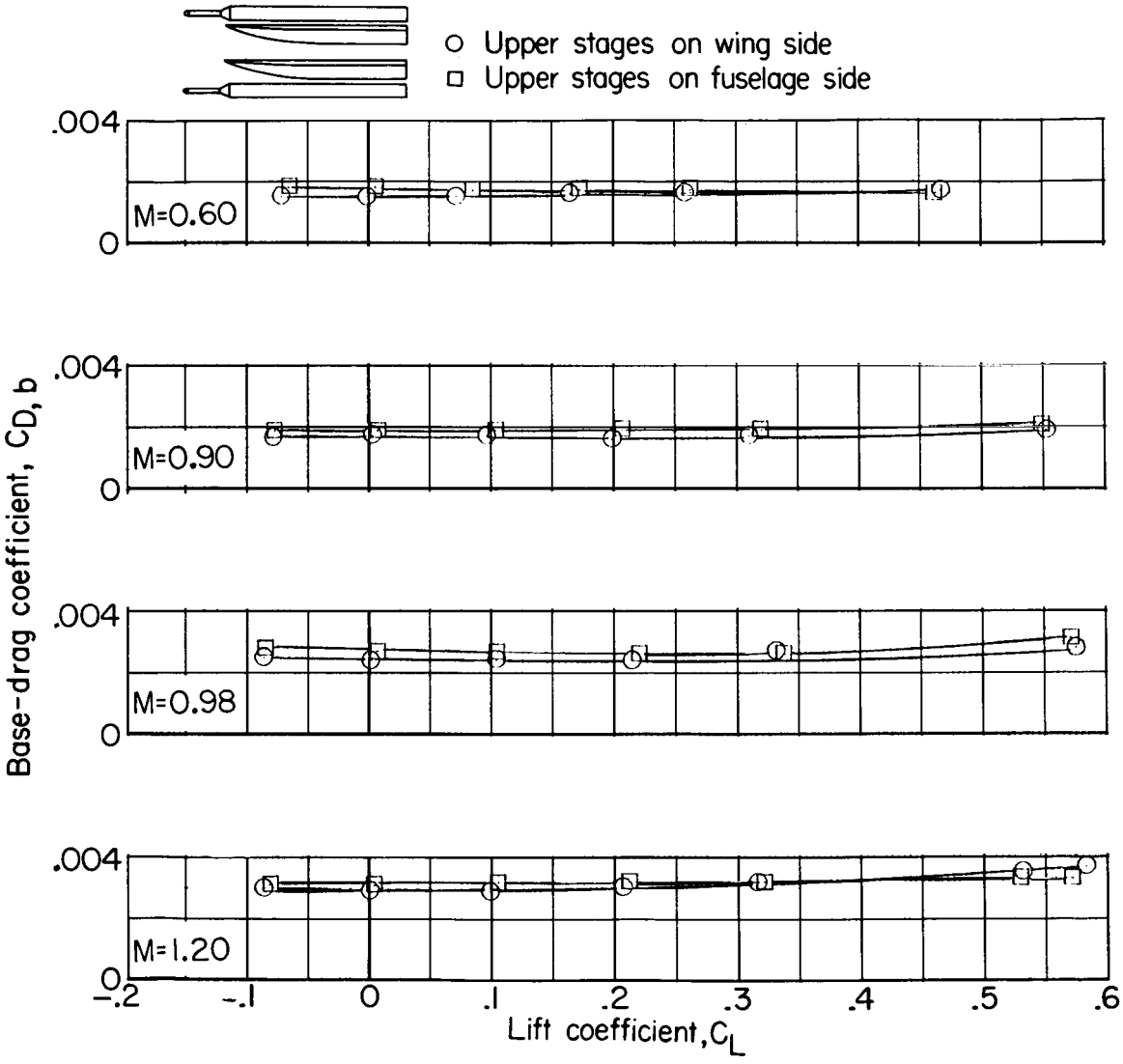

(d) Variation of base-drag coefficient with lift coefficient.

Figure 6.- Concluded.

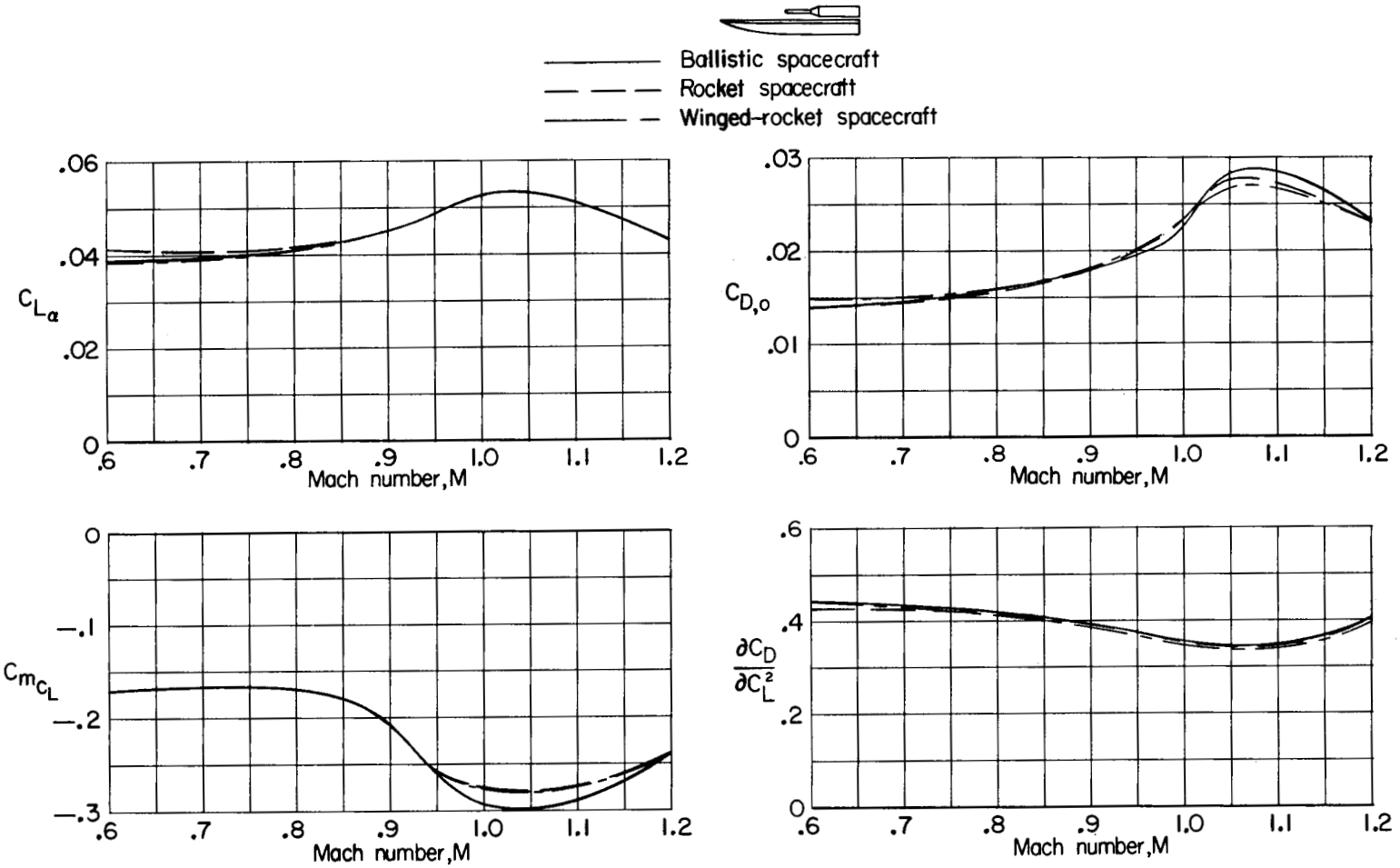

Figure 7.- Variation with Mach number of the longitudinal-stability and drag parameters for the several spacecraft attached to a one-stage rocket booster mounted on top of the high-wing recoverable booster.

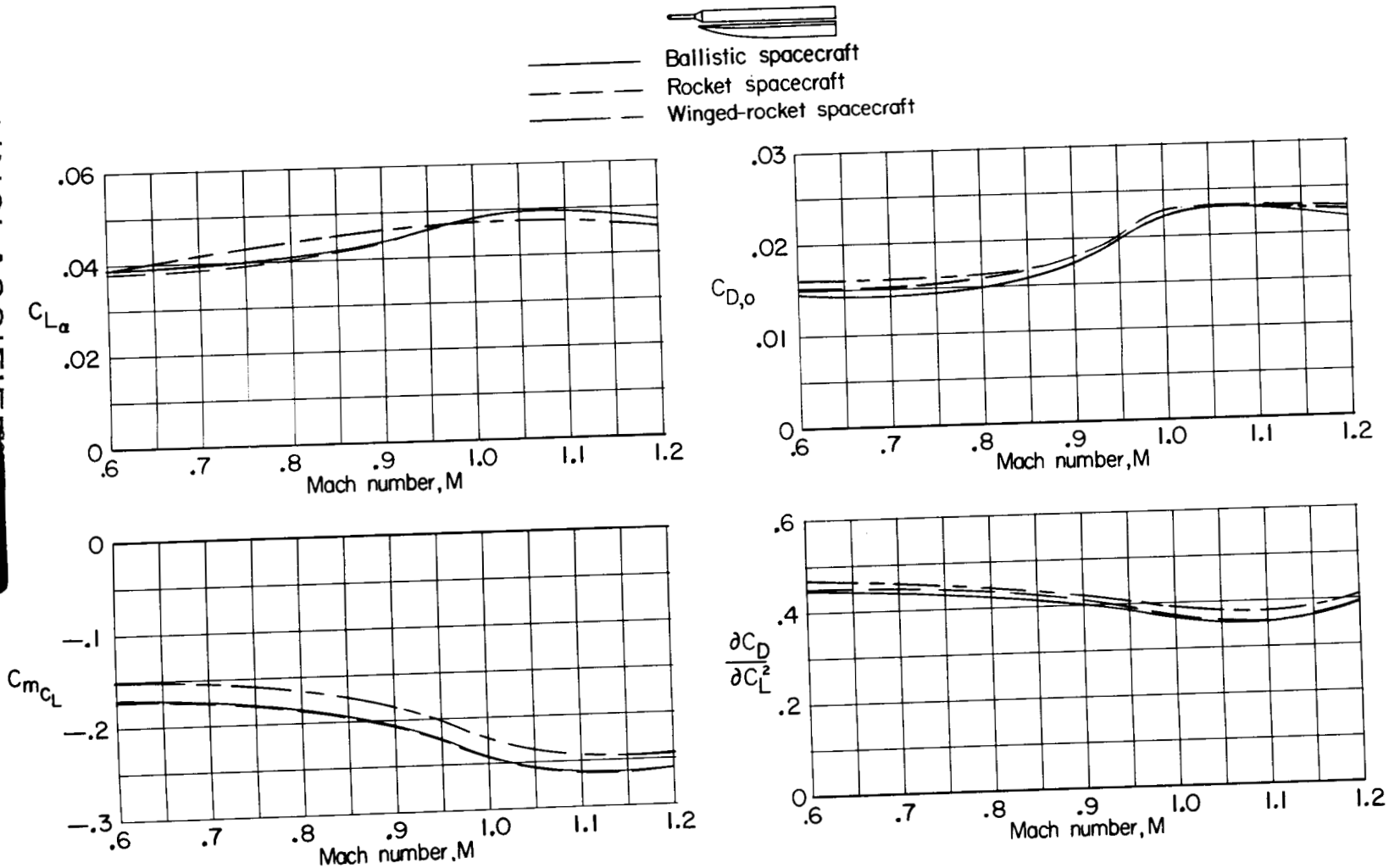

Figure 8.- Variation with Mach number of the longitudinal-stability and drag parameters for the several spacecraft attached to a two-stage rocket booster mounted on top of the high-wing recoverable booster.

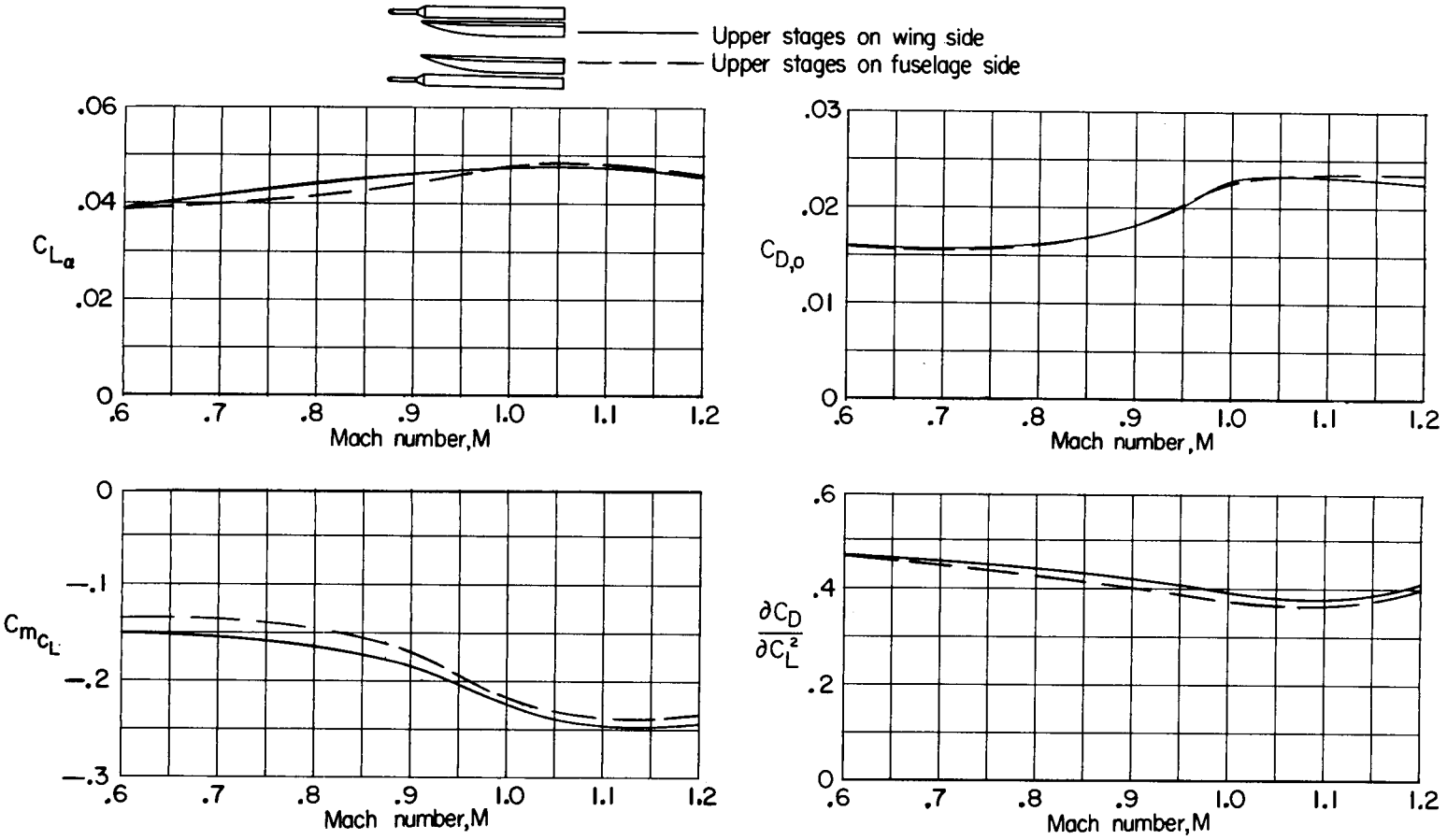

Figure 9.- Variation with Mach number of the longitudinal-stability and drag parameters for the winged-rocket spacecraft attached to the two-stage rocket booster mounted above or beneath the high-wing recoverable booster.

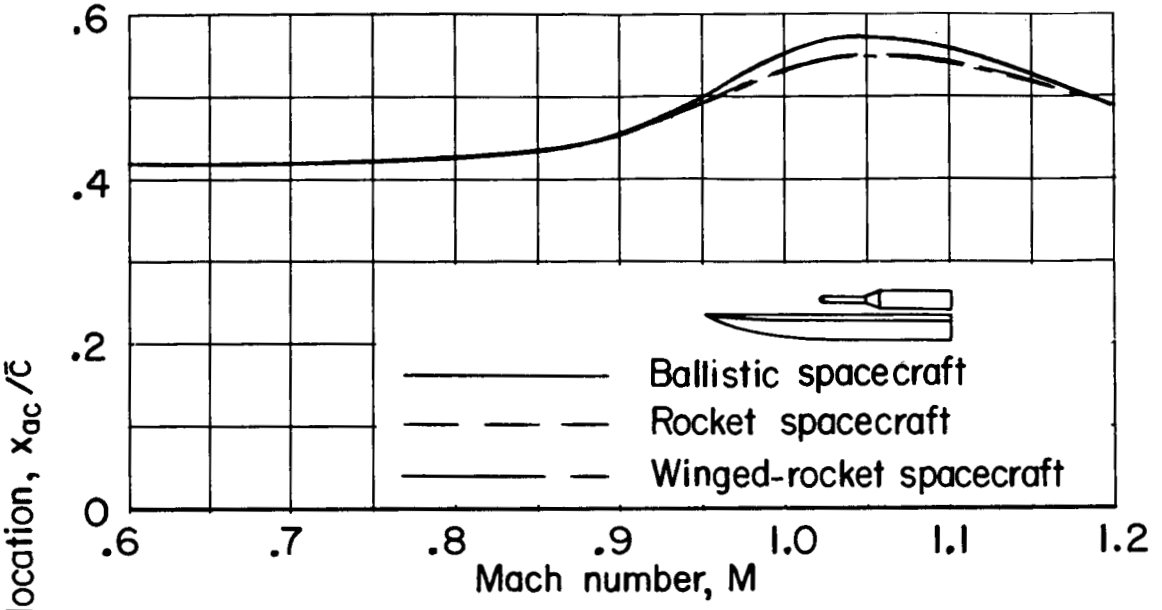

(a) With one-stage rocket booster.

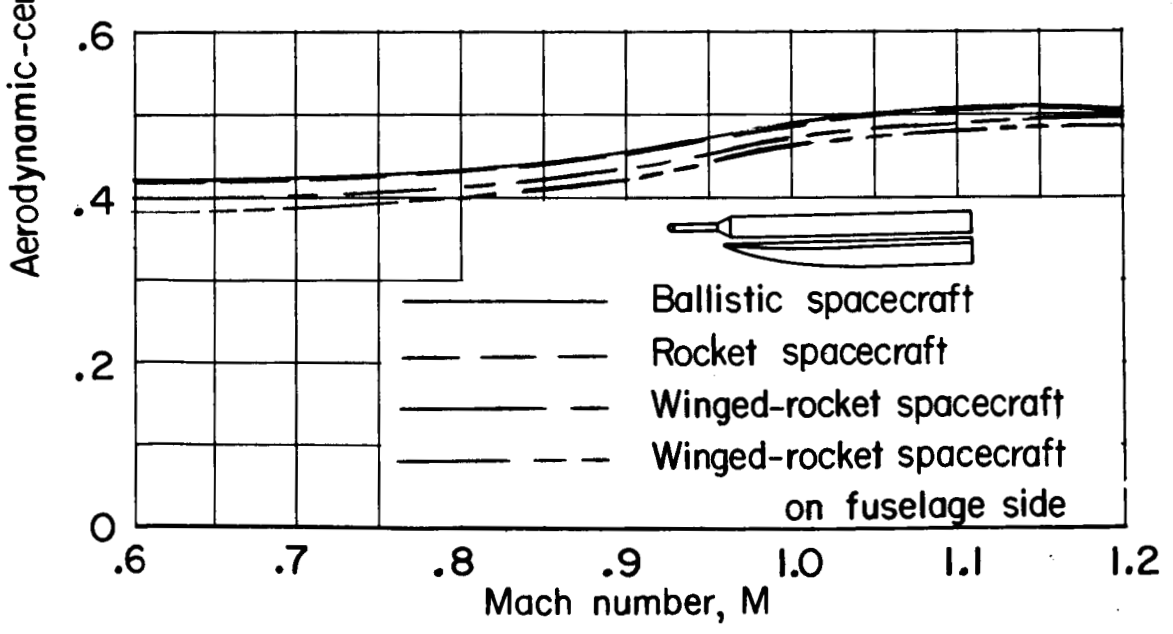

(b) With two-stage rocket booster.

Figure 10.- Variation of the aerodynamic-center location with Mach number for the several upper stages mounted on top of the high-wing recoverable booster.

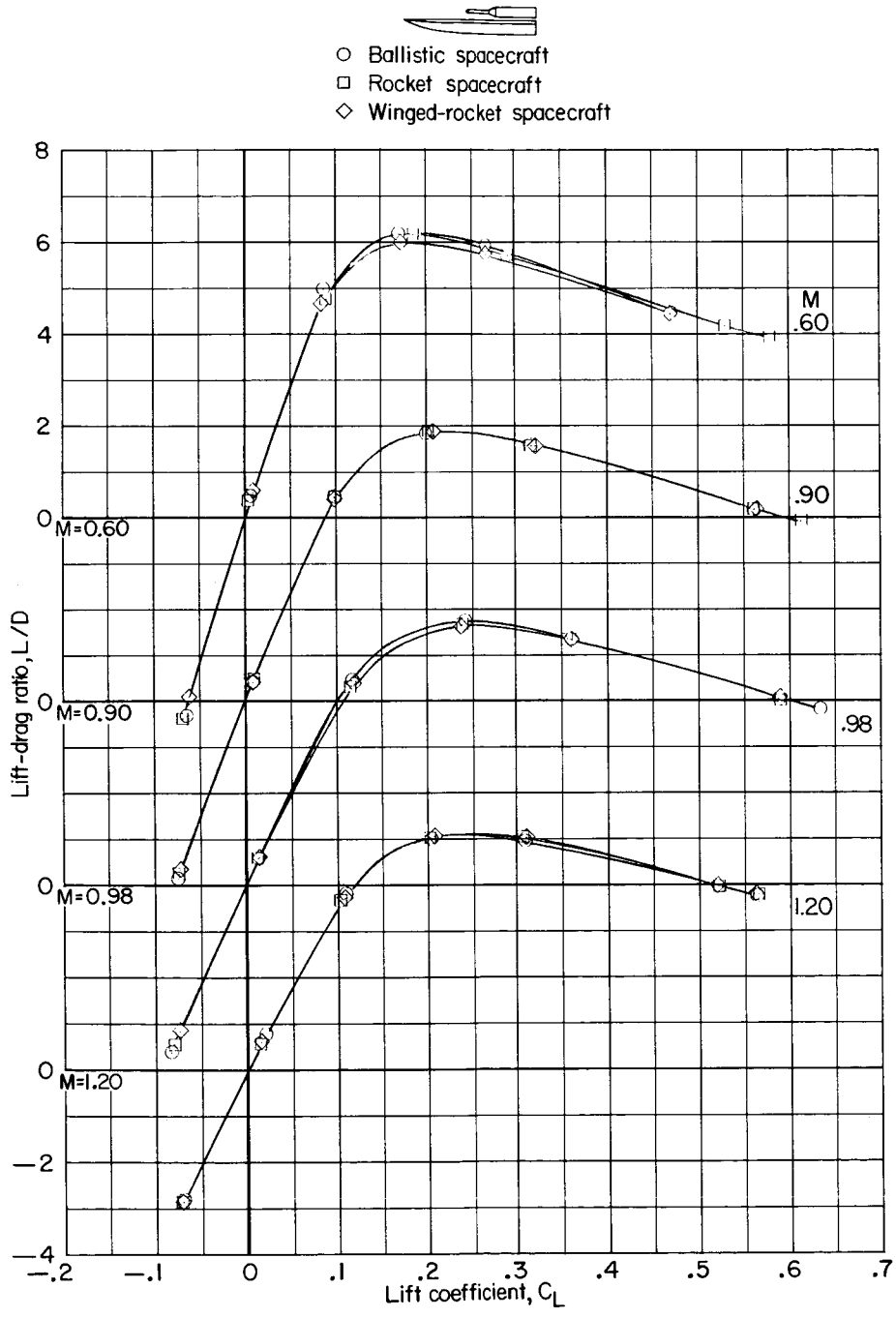

(a) With one-stage rocket booster.

Figure 11.- Variation of the lift-drag ratio with lift coefficient for the several upper stages mounted on top of the high-wing recoverable booster.

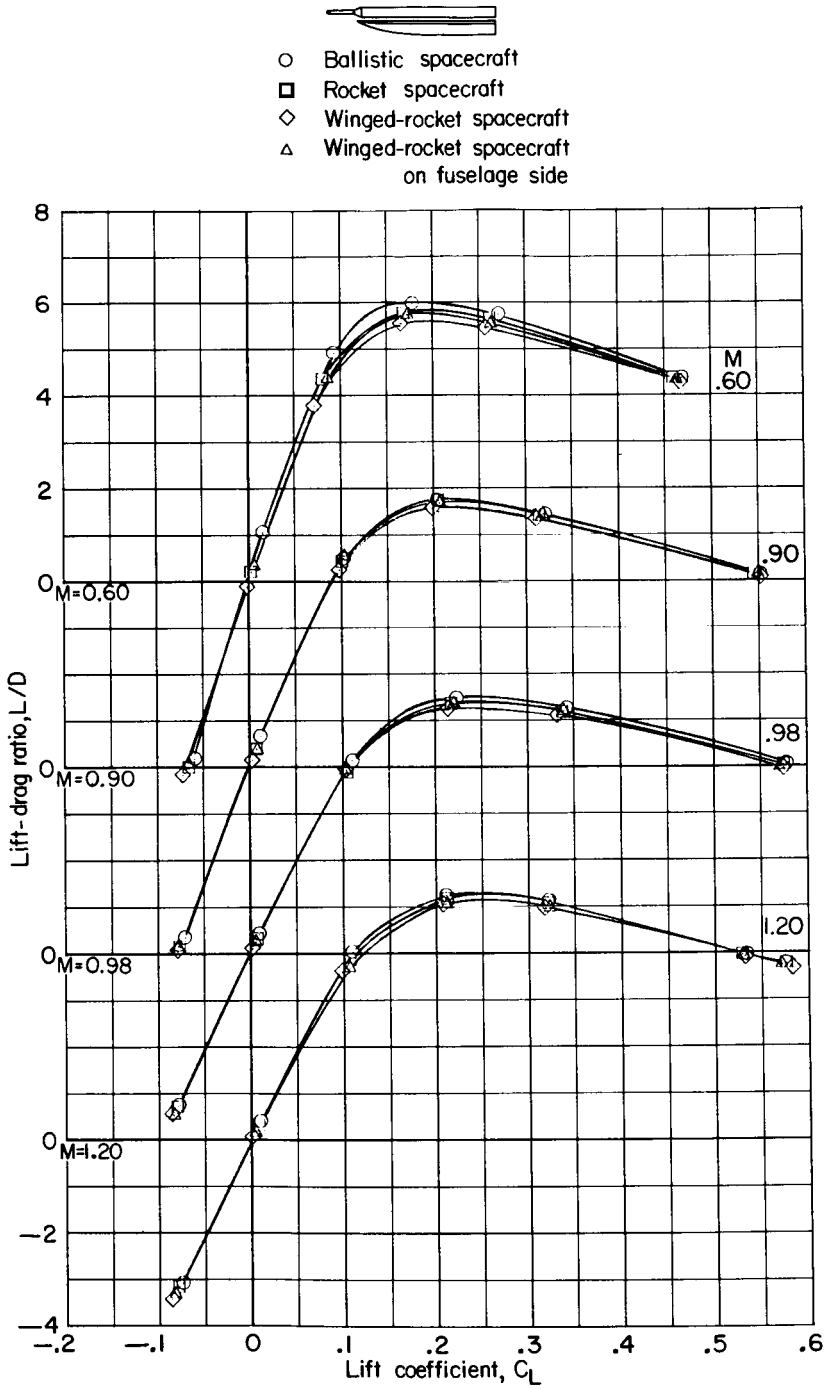

(b) With two-stage rocket booster.

Figure 11.- Concluded.

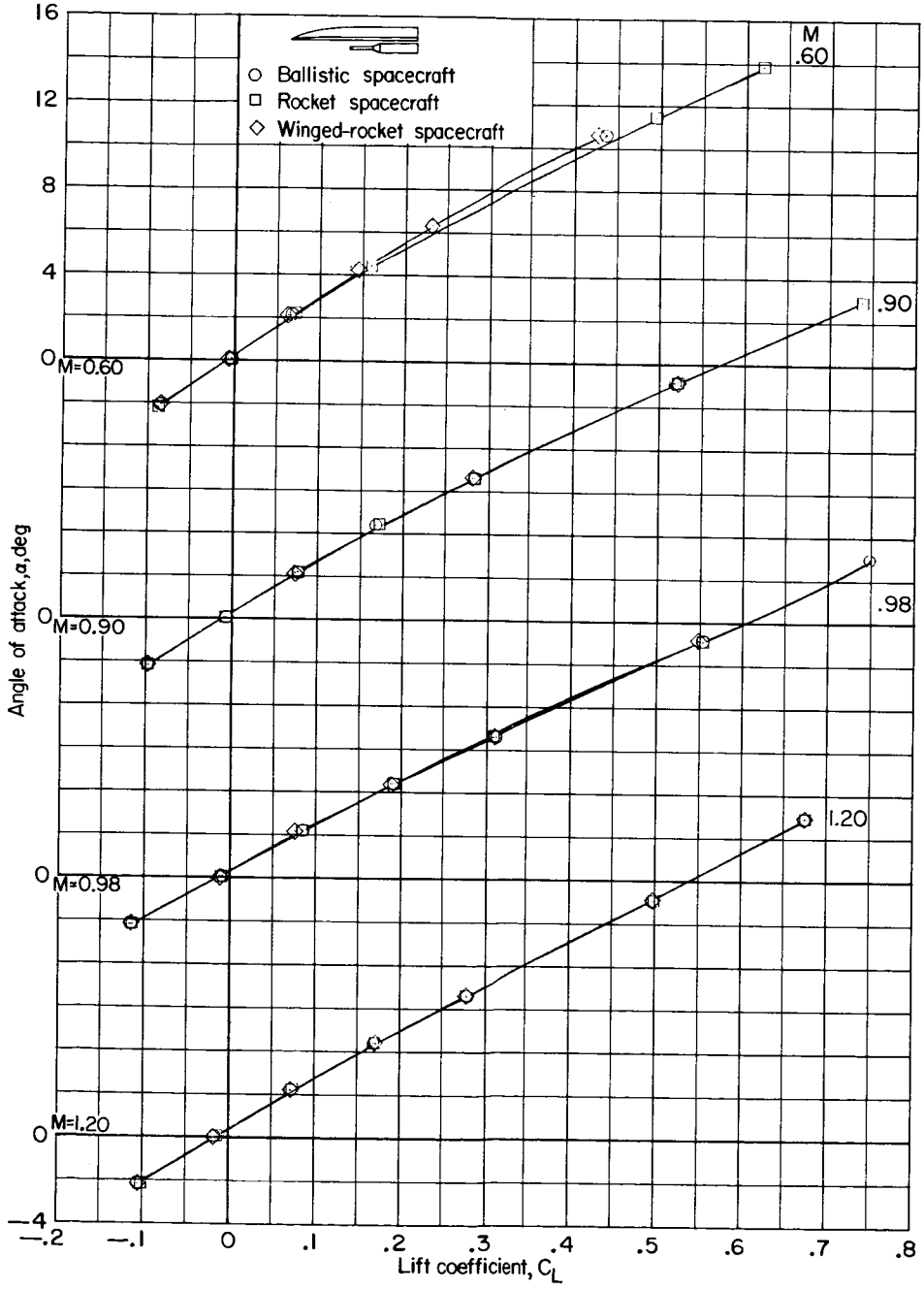

(a) Variation of lift coefficient with angle of attack.

Figure 12.- Aerodynamic characteristics of the several spacecraft attached to a one-stage rocket booster mounted beneath the low-wing recoverable booster.

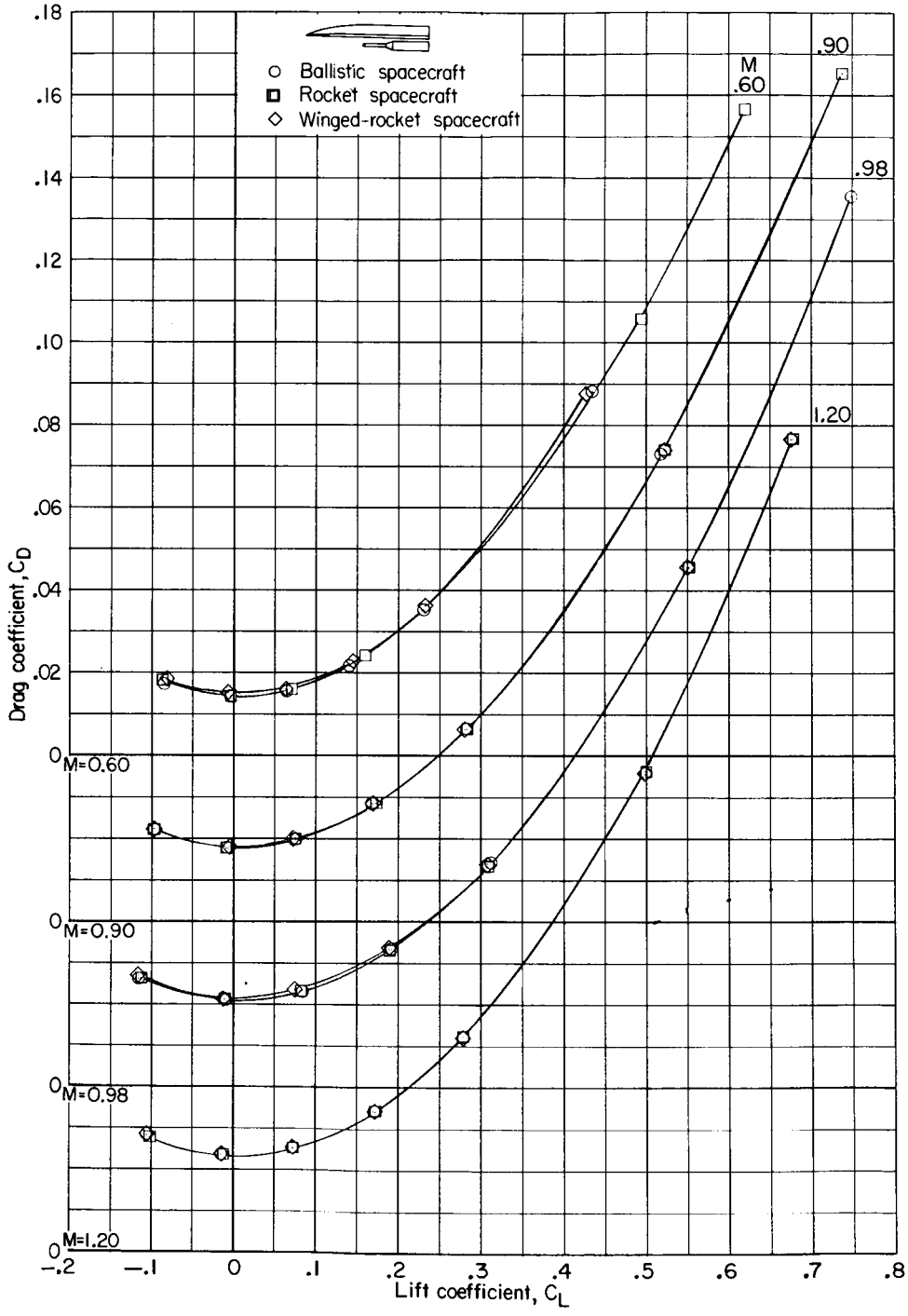

(b) Variation of drag coefficient with lift coefficient.

Figure 12.- Continued.

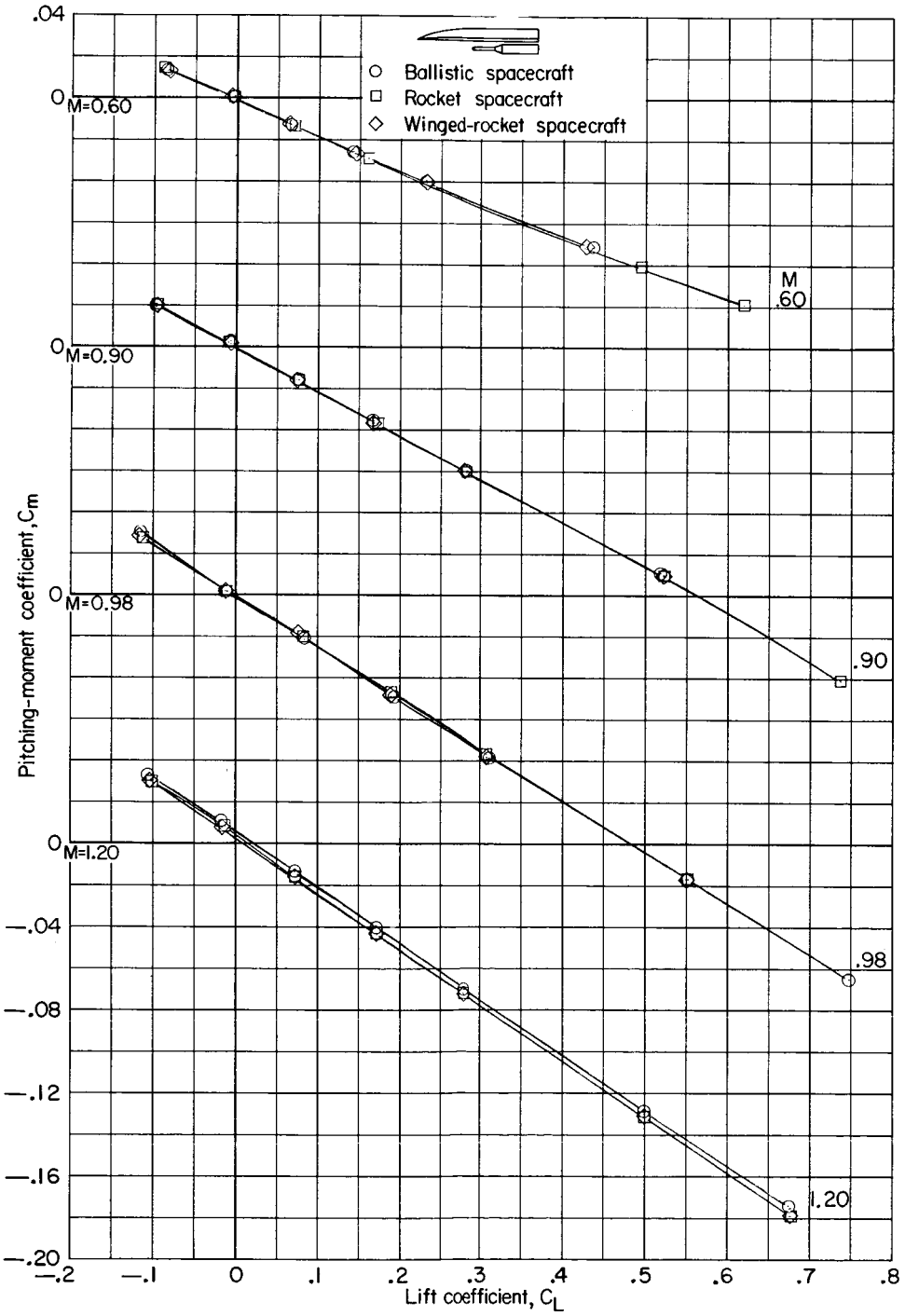

(c) Variation of pitching-moment coefficient with lift coefficient.

Figure 12.- Continued.

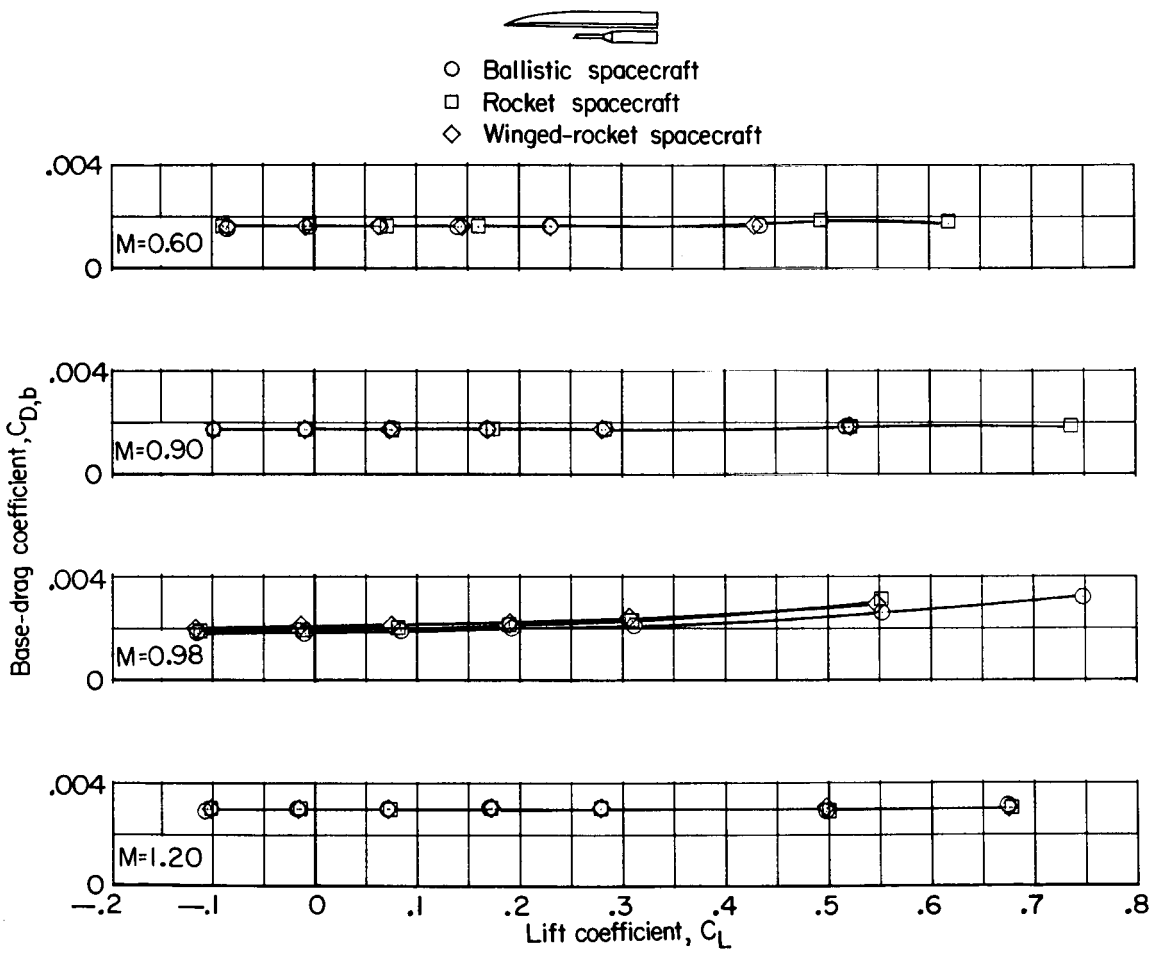

(d) Variation of base-drag coefficient with lift coefficient.

Figure 12.- Concluded.

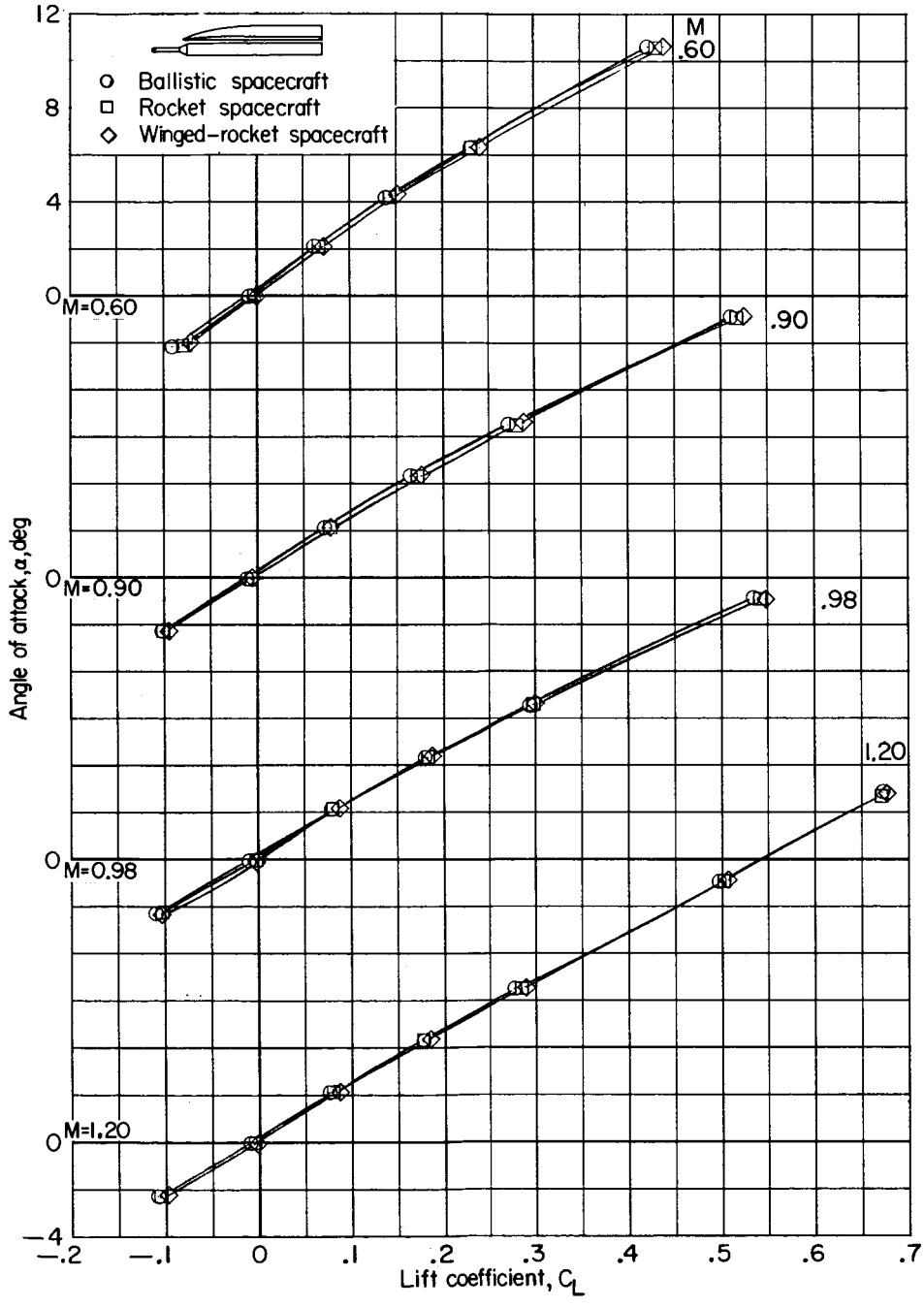

(a) Variation of lift coefficient with angle of attack.

Figure 13.- Aerodynamic characteristics of the several spacecraft attached to a two-stage rocket booster mounted beneath the low-wing recoverable booster.

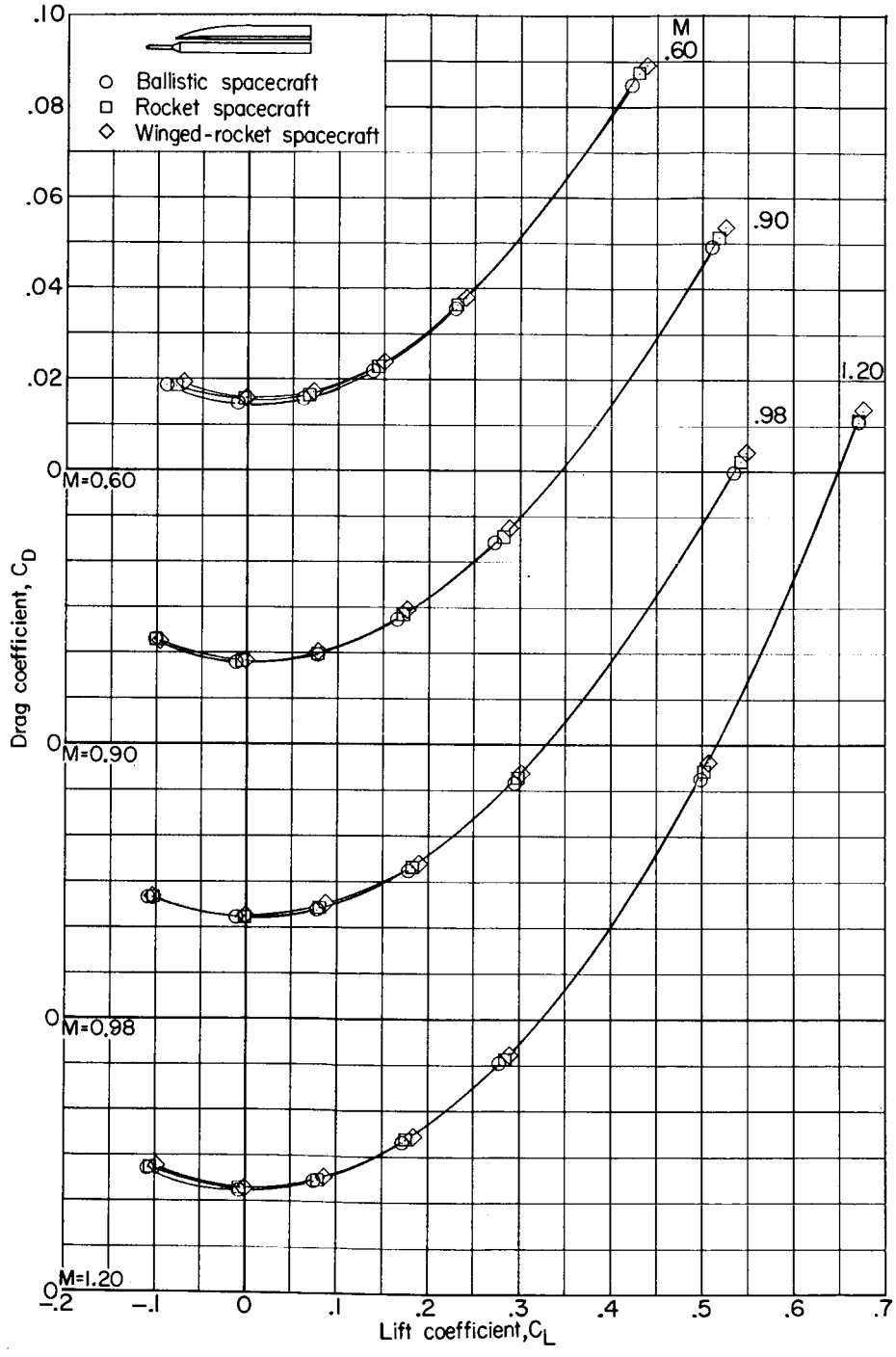

(b) Variation of drag coefficient with lift coefficient.

Figure 13.- Continued.

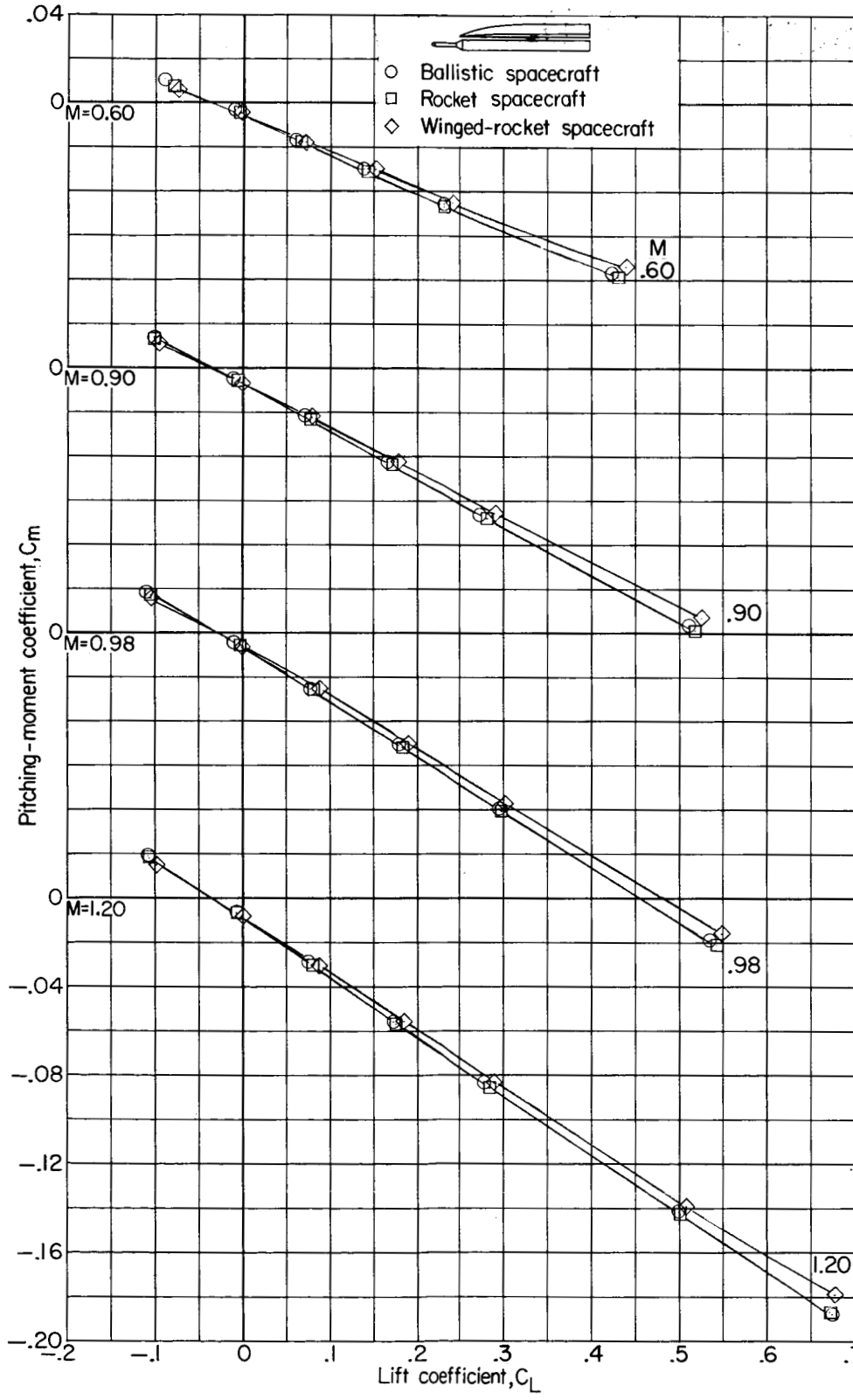

(c) Variation of pitching-moment coefficient with lift coefficient.

Figure 13.- Continued.

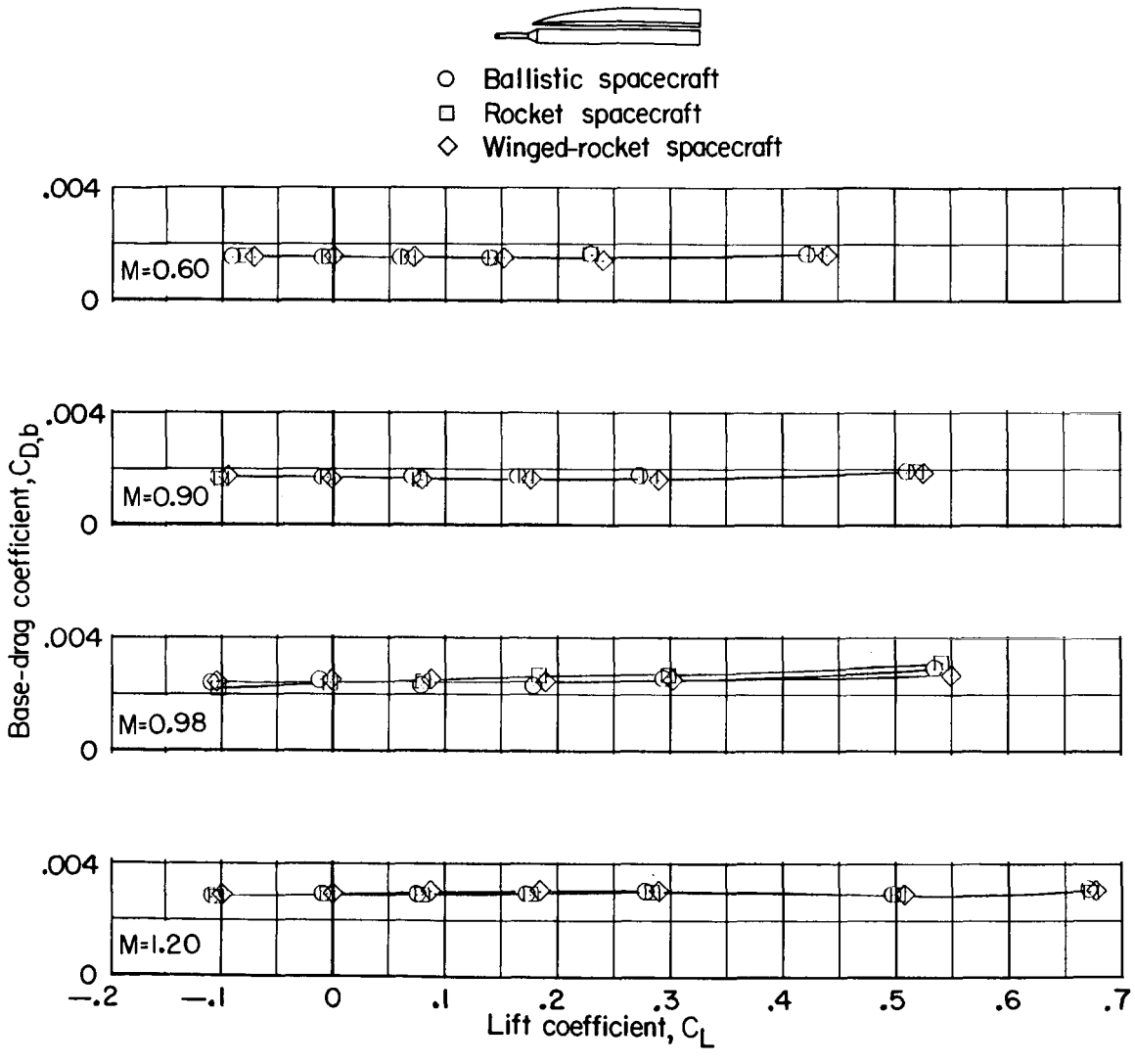

(d) Variation of base-drag coefficient with lift coefficient.

Figure 13.- Concluded.

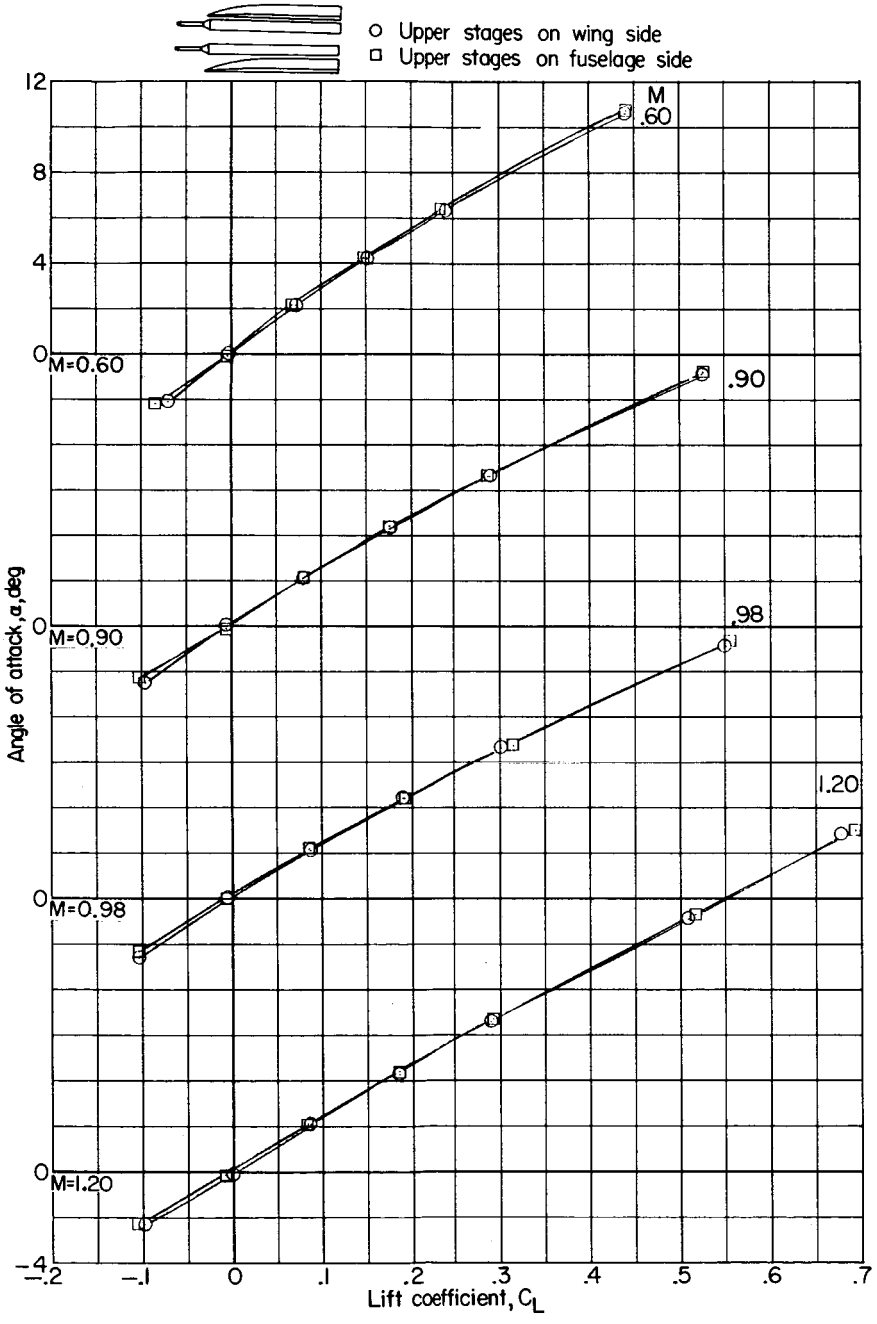

(a) Variation of lift coefficient with angle of attack.

Figure 14.- Aerodynamic characteristics of the winged-rocket spacecraft attached to a two-stage rocket booster mounted above or beneath the low-wing recoverable booster.

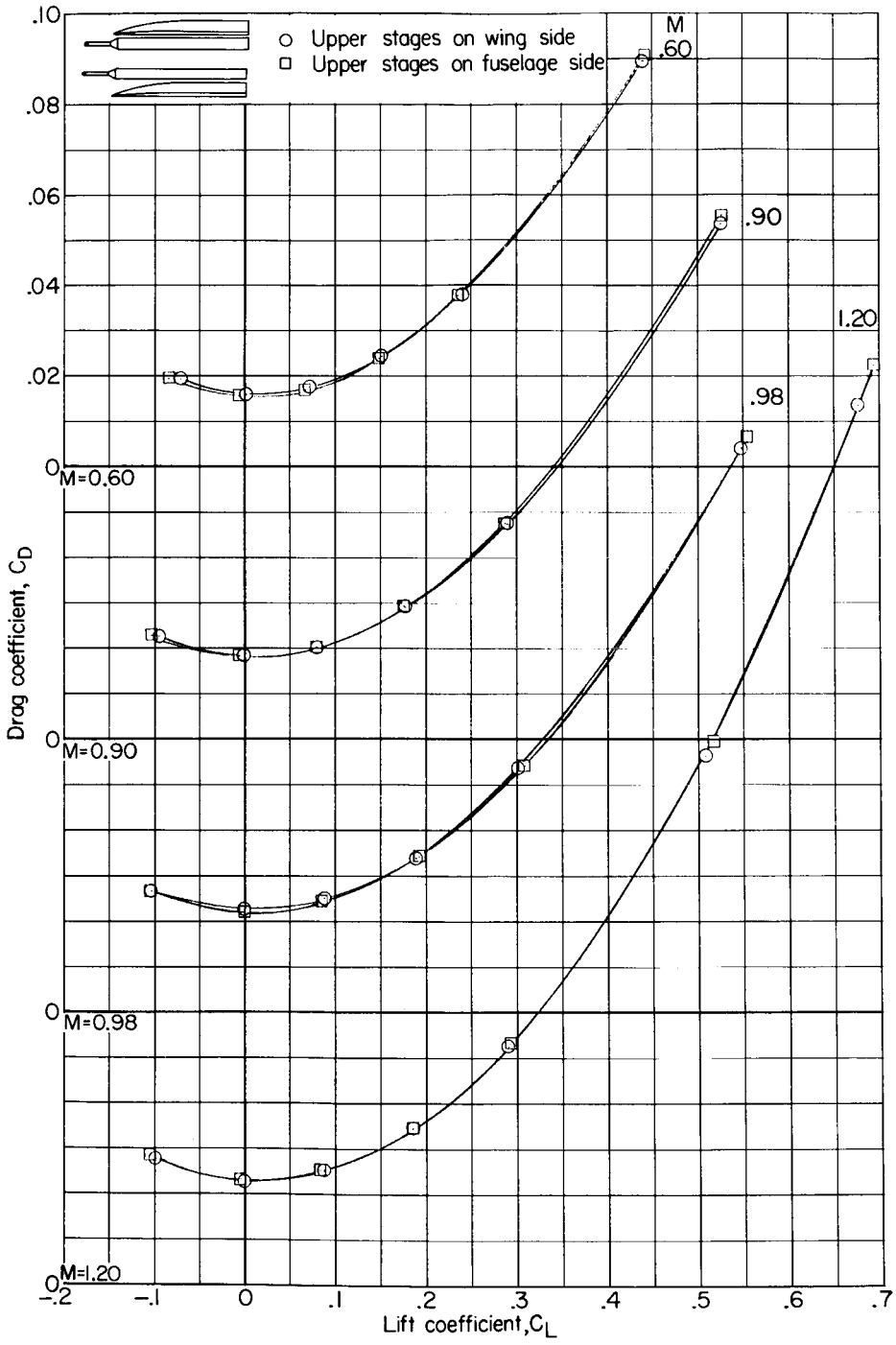

(b) Variation of drag coefficient with lift coefficient.

Figure 14.- Continued.

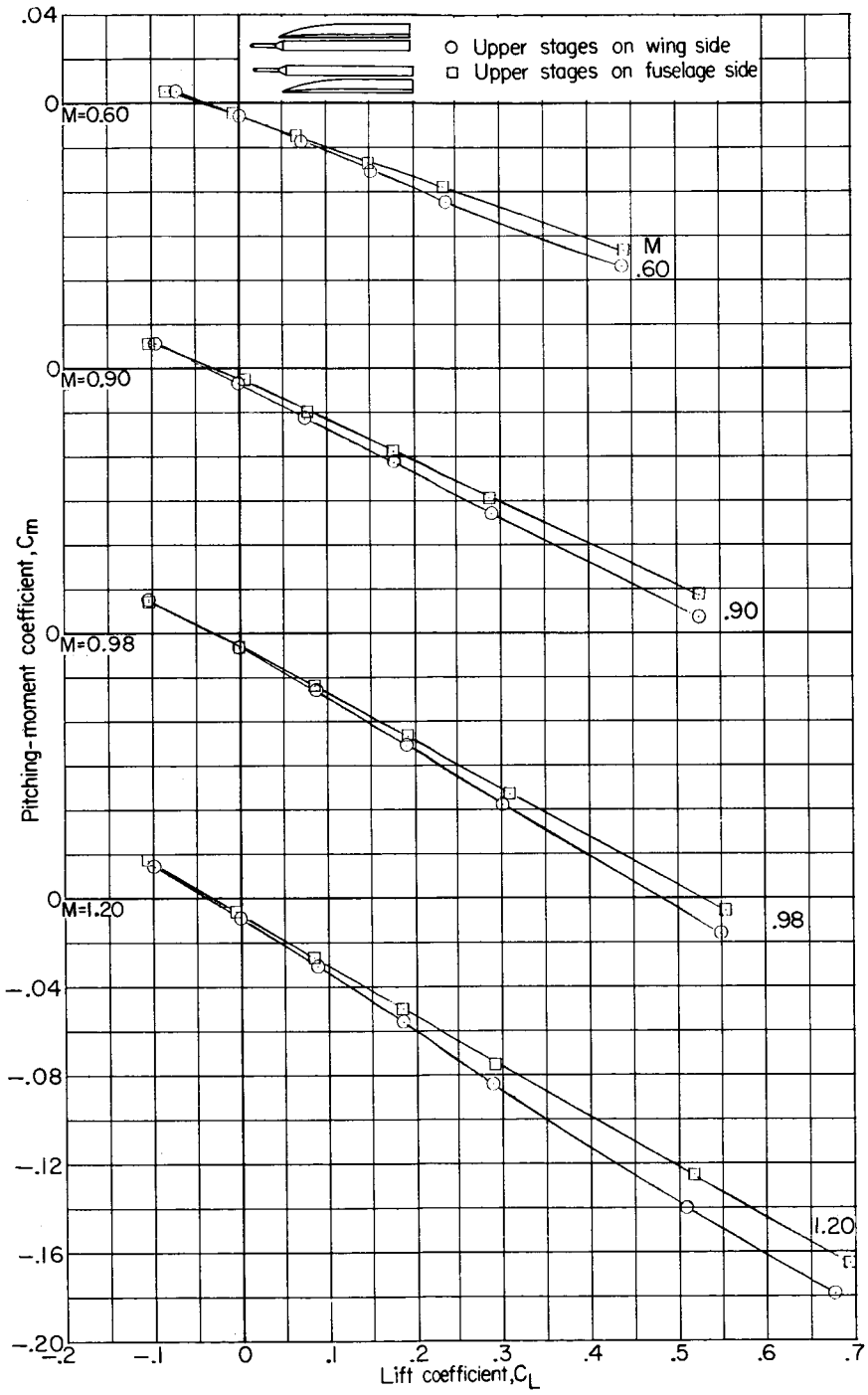

(c) Variation of pitching-moment coefficient with lift coefficient.

Figure 14.- Continued.

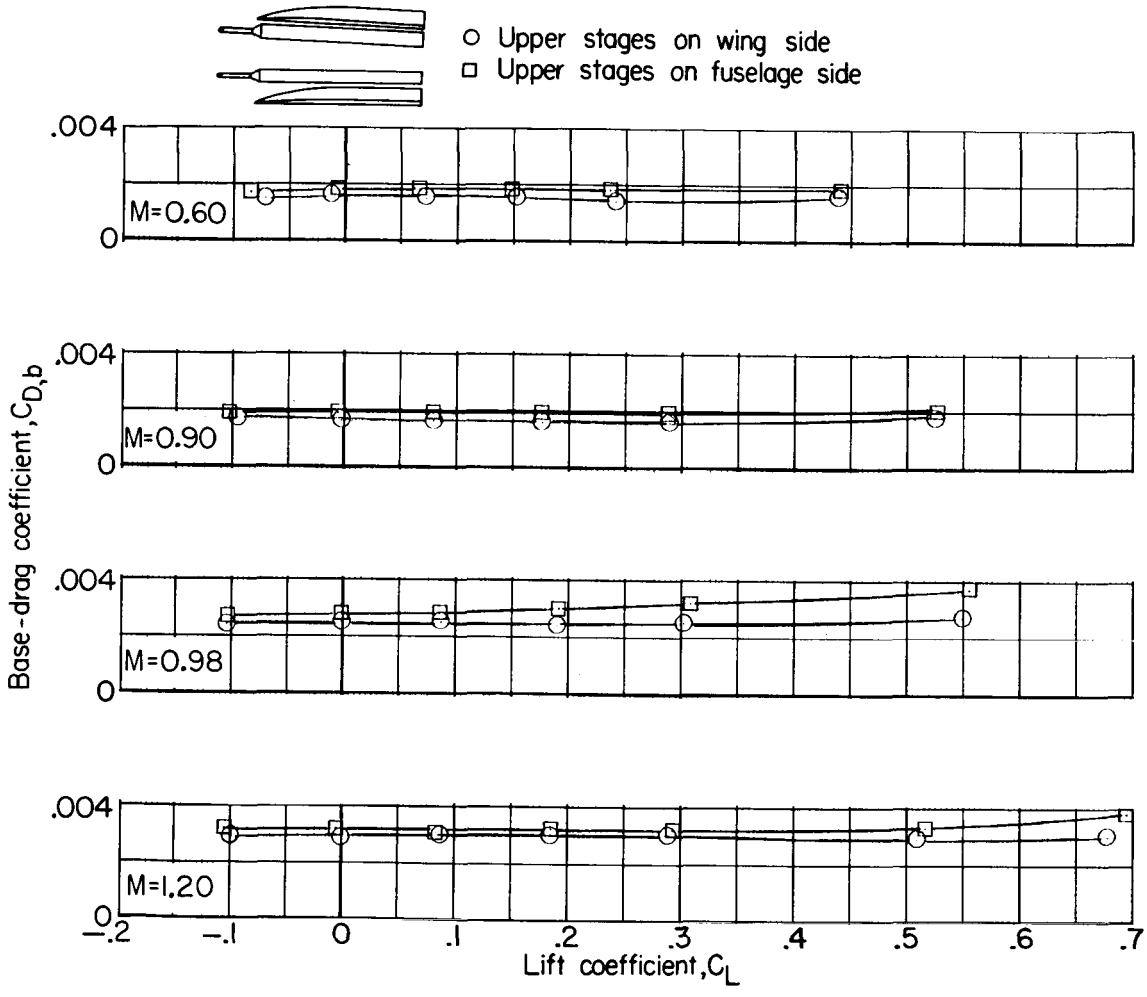

(d) Variation of base-drag coefficient with lift coefficient.

Figure 14.- Concluded.

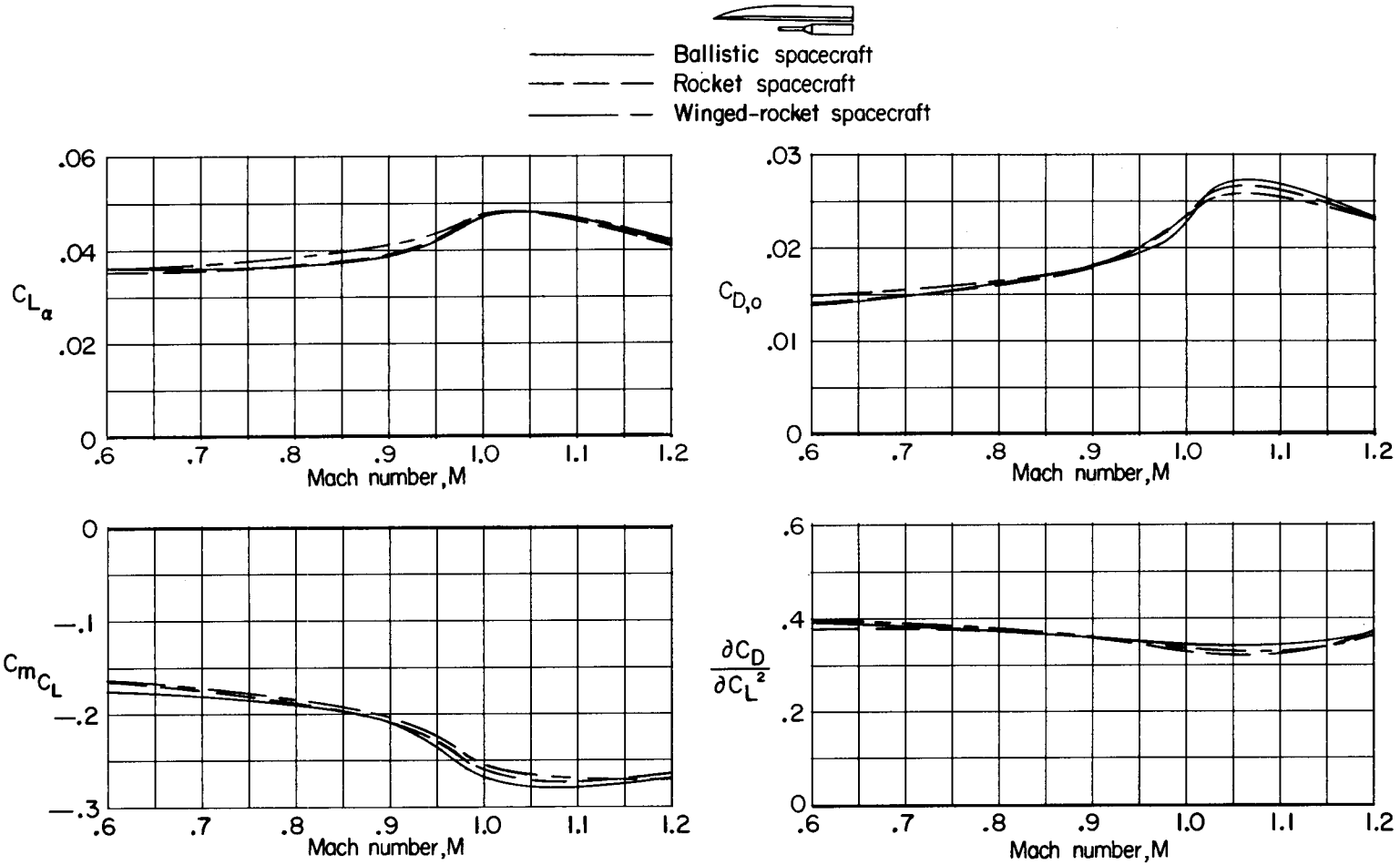

Figure 15.- Variation with Mach number of the longitudinal-stability and drag parameters for the several spacecraft attached to a one-stage rocket booster mounted beneath the low-wing recoverable booster.

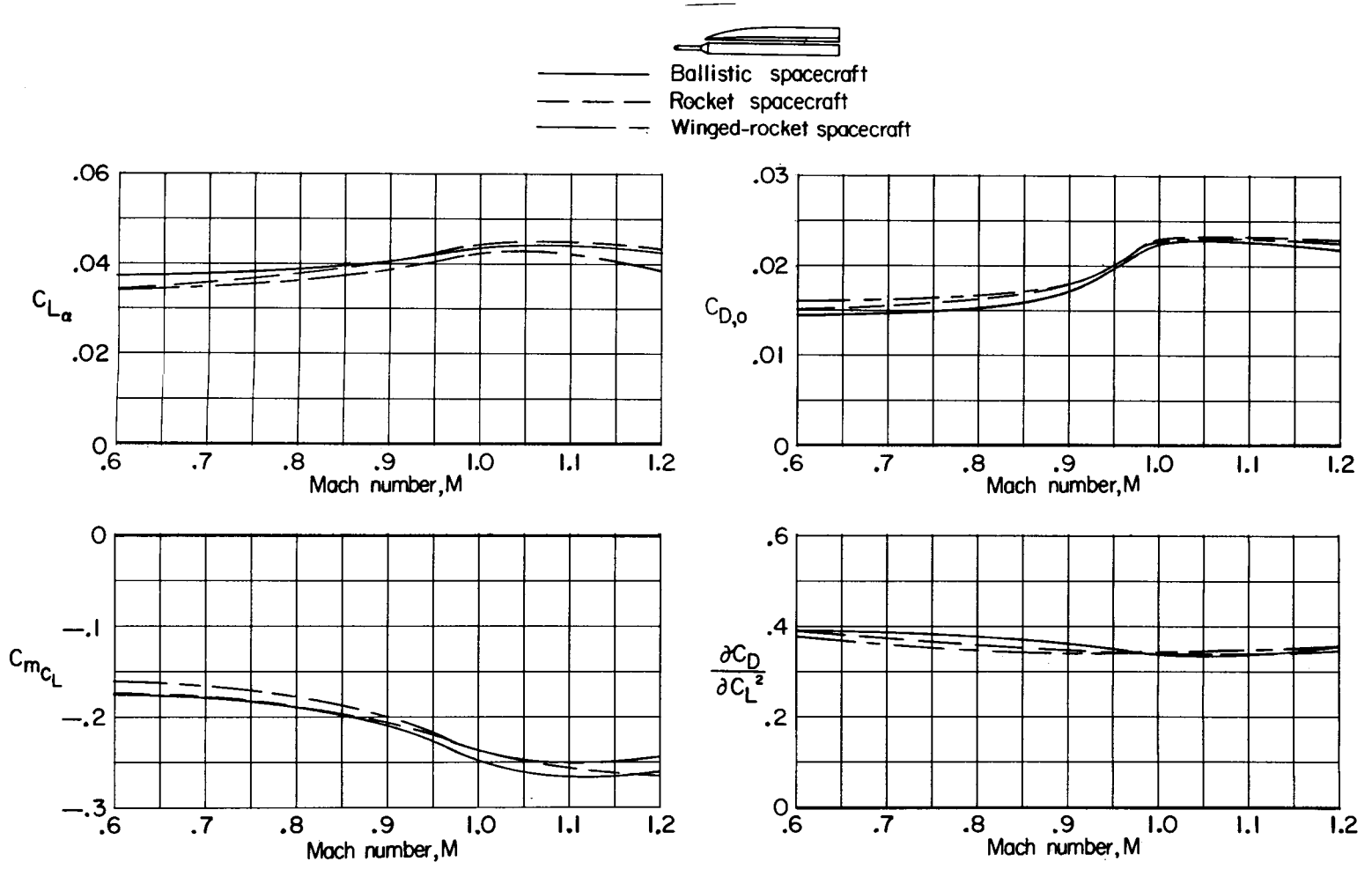

Figure 16.- Variation with Mach number of the longitudinal-stability and drag parameters for the several spacecraft attached to a two-stage rocket booster mounted beneath the low-wing recoverable booster.

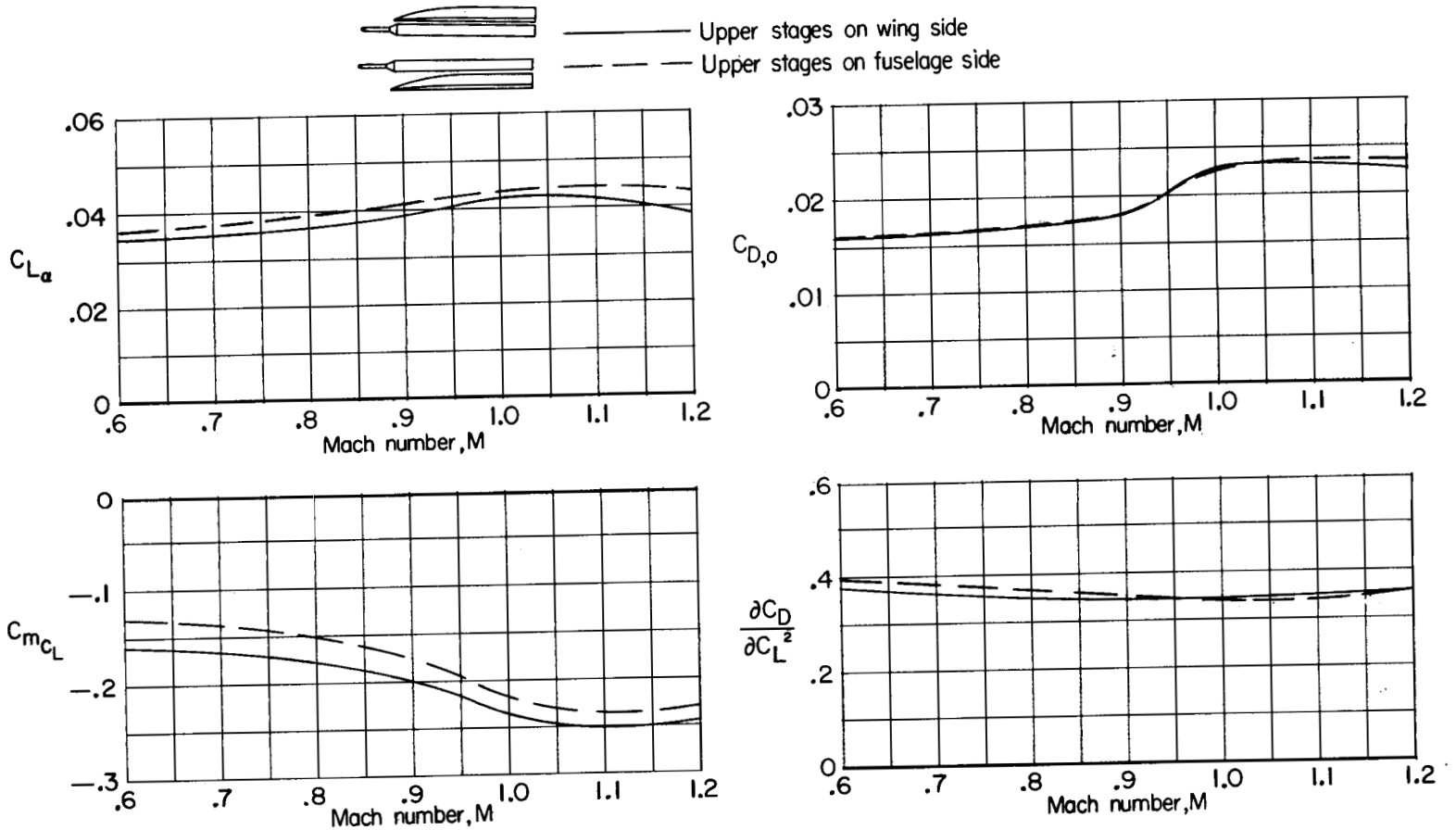

Figure 17.- Variation with Mach number of the longitudinal-stability and drag parameters for the winged-rocket spacecraft attached to the two-stage rocket booster mounted above or beneath the low-wing recoverable booster.

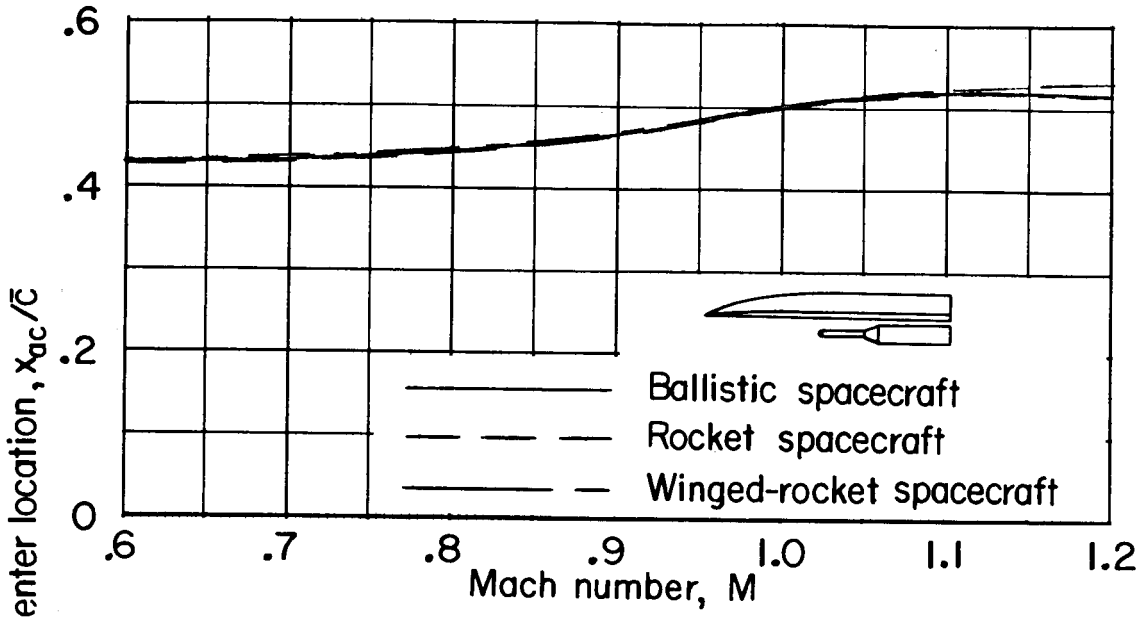

(a) With one-stage rocket booster.

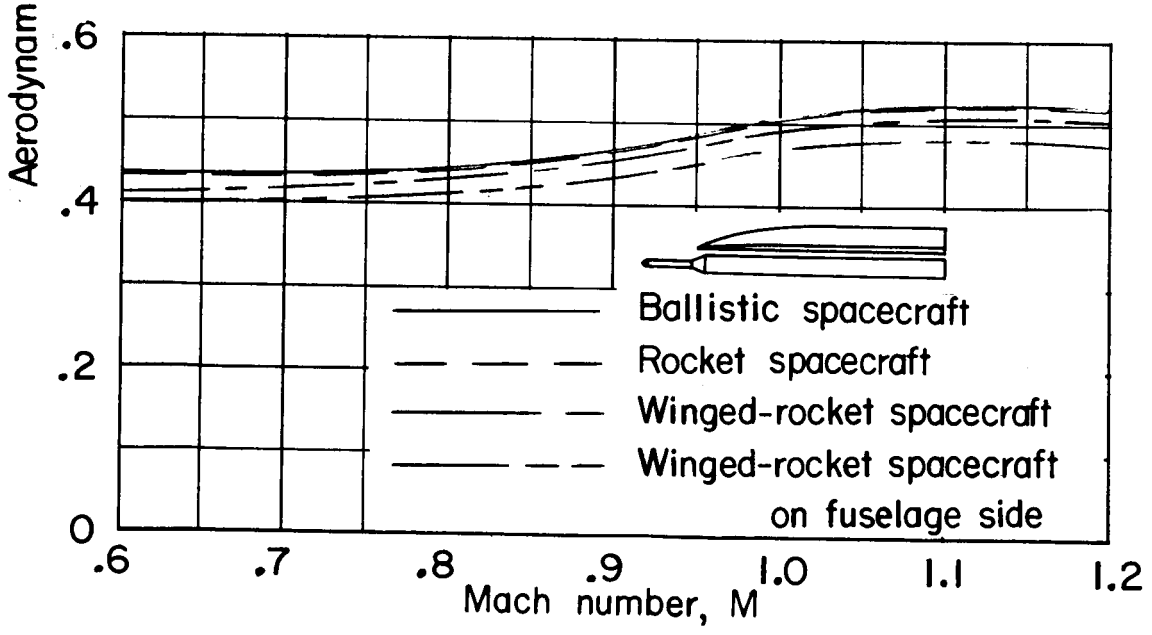

(b) With two-stage rocket booster.

Figure 18.- Variation of the aerodynamic-center location with Mach number for the several upper stages mounted beneath the low-wing recoverable booster.

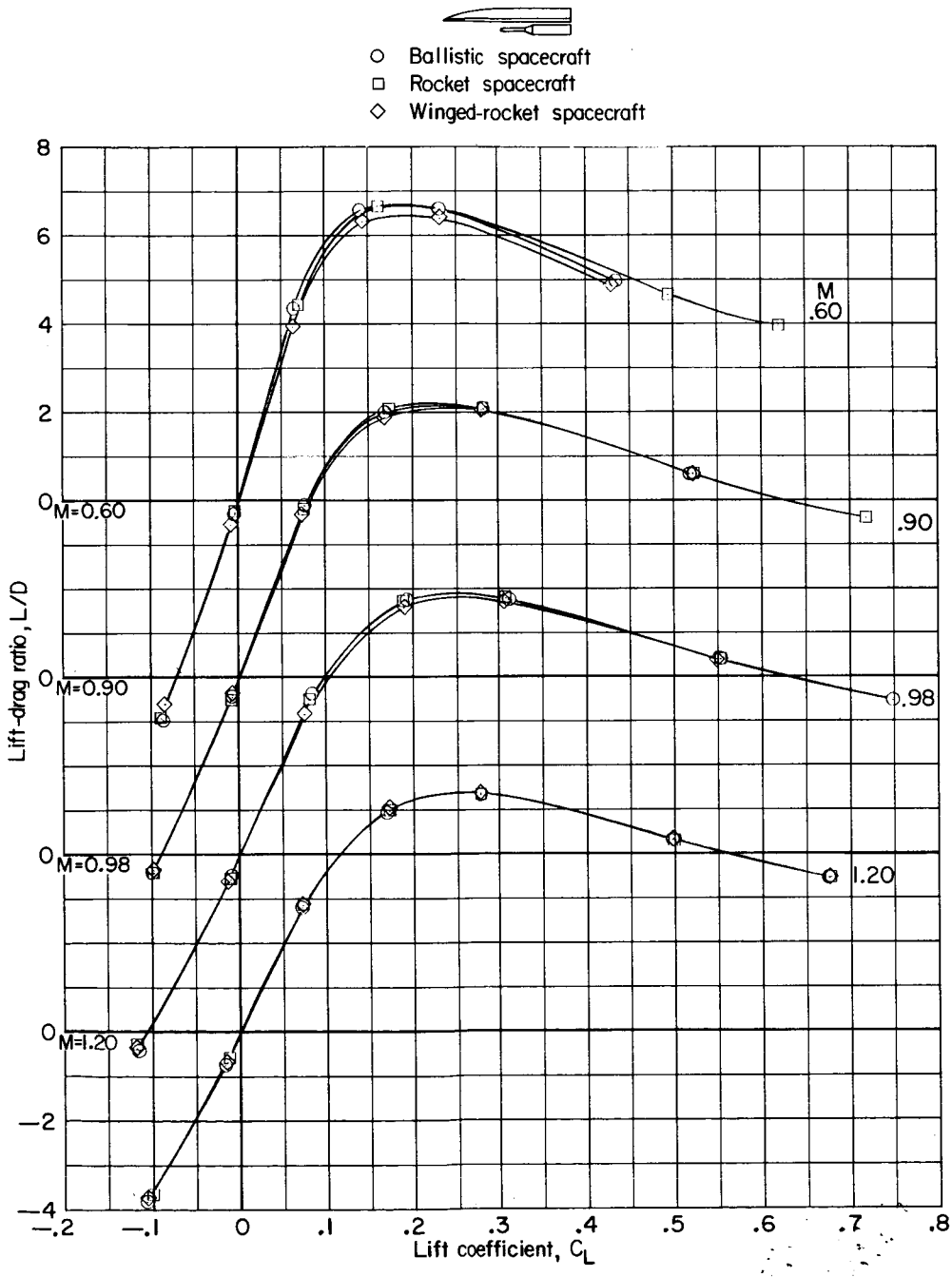

(a) With one-stage rocket booster.

Figure 19.- Variation of the lift-drag ratio with lift coefficient for the several upper stages mounted beneath the low-wing recoverable booster.

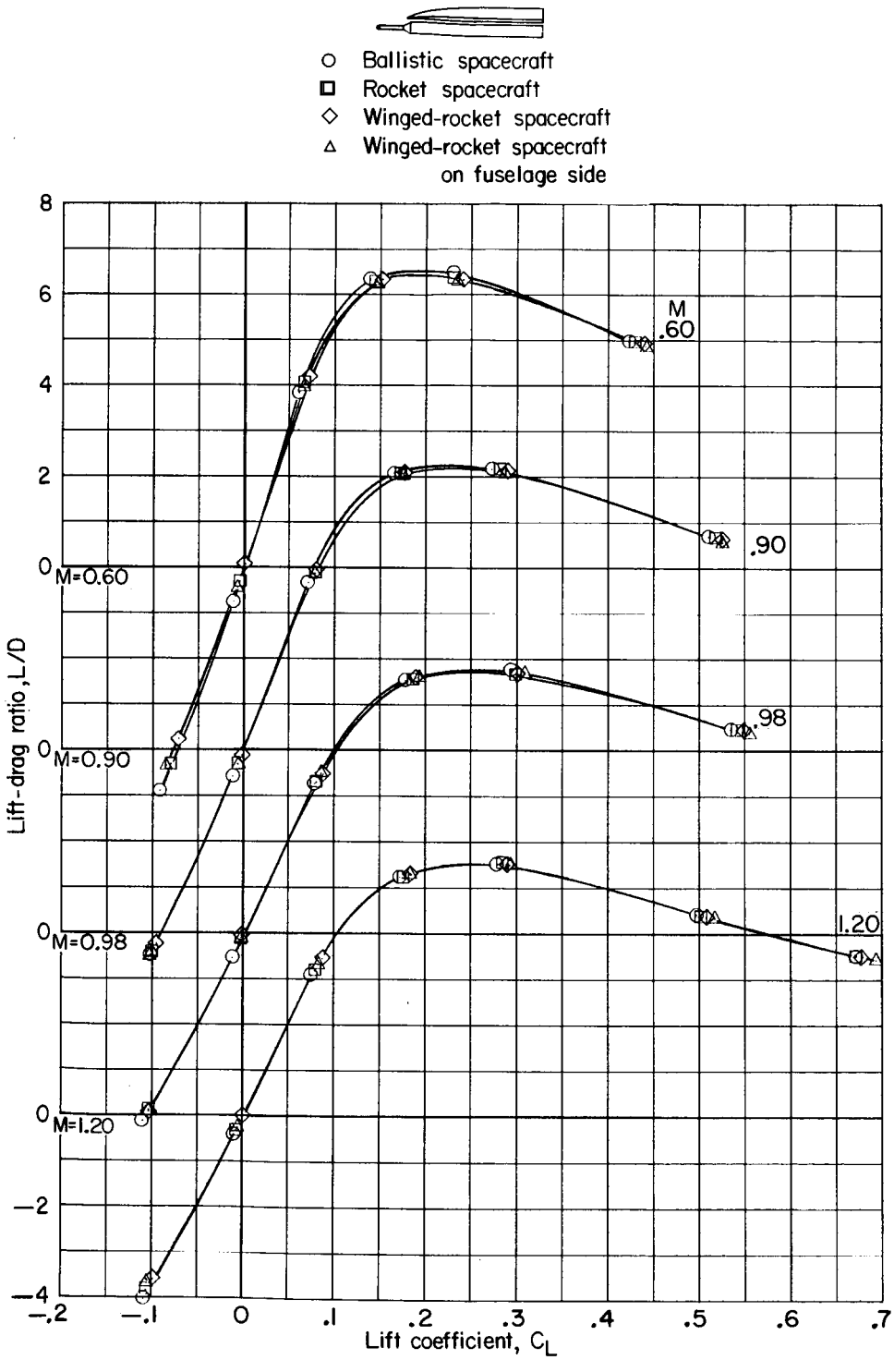

(b) With two-stage rocket booster.

Figure 19.- Concluded.

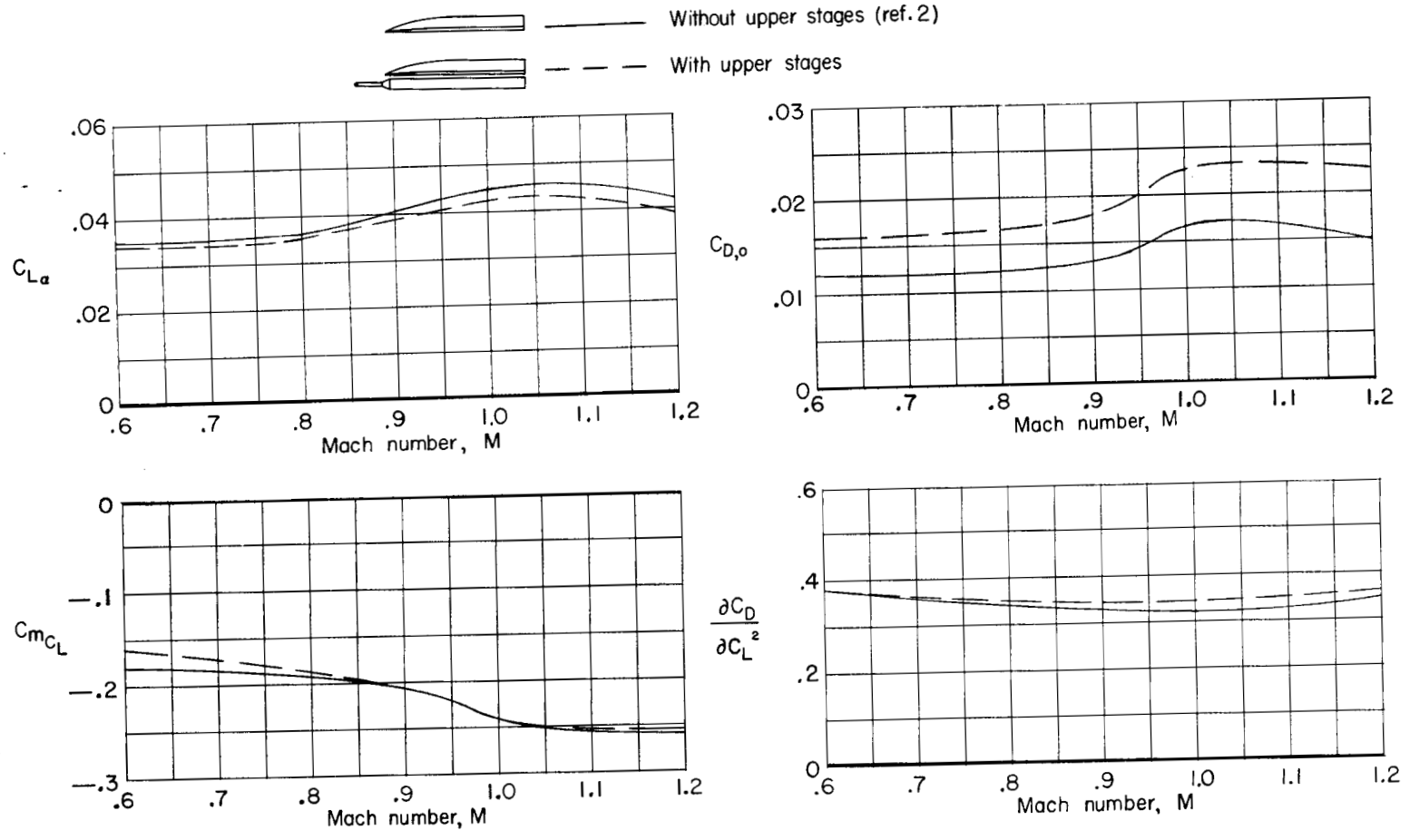

Figure 20.- Variation with Mach number of the longitudinal-stability parameter and zero-lift drag coefficient for the low-wing recoverable booster without and with a two-stage rocket booster and winged-rocket spacecraft mounted beneath the wing.

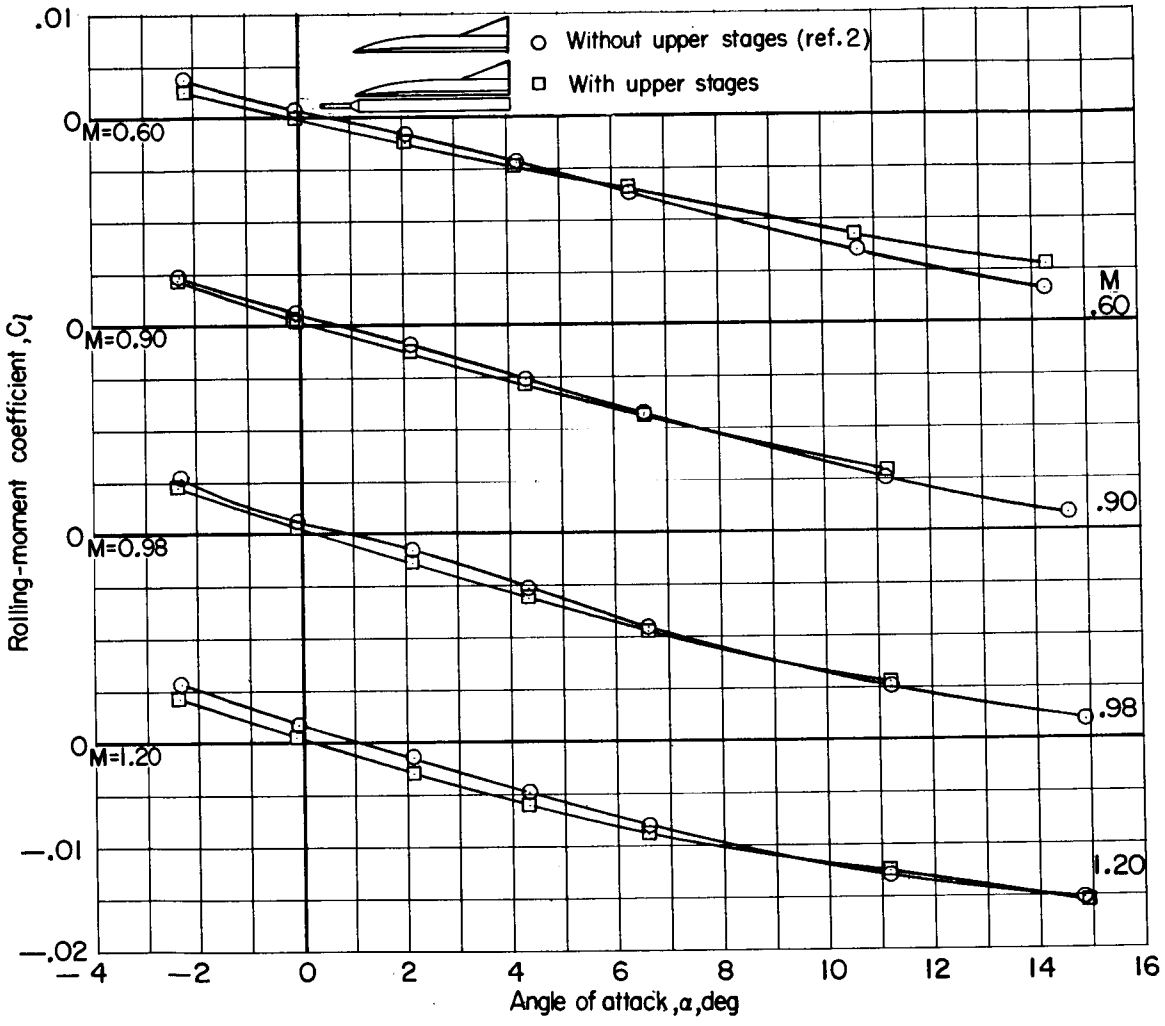

(a) Variation of rolling-moment coefficient with angle of attack.

Figure 21.- Aerodynamic characteristics for the low-wing recoverable booster without and with a two-stage rocket booster and winged-rocket spacecraft mounted beneath the wing. $\beta = 5^{\circ}$.

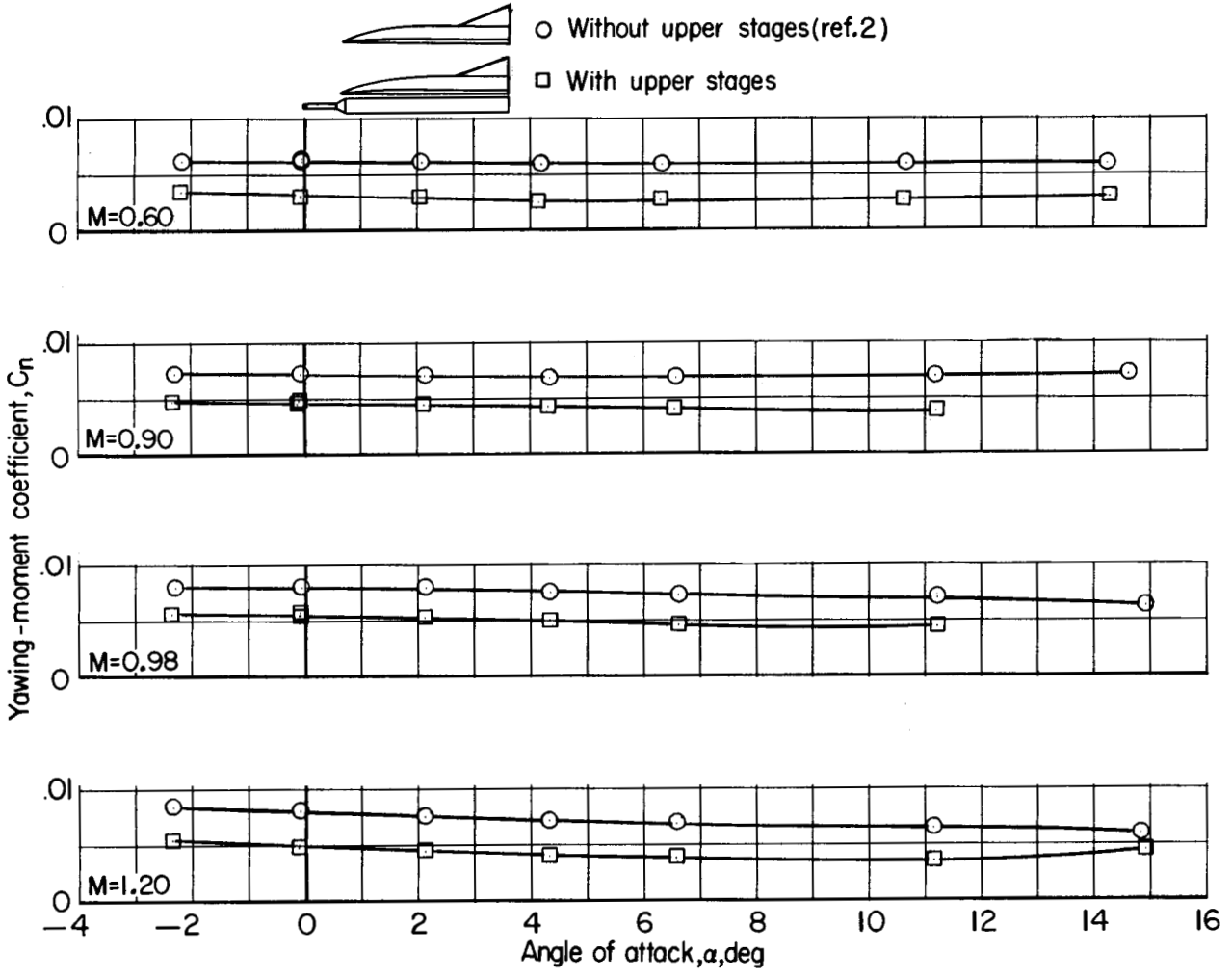

(b) Variation of yawing-moment coefficient with angle of attack.

Figure 21.- Continued.

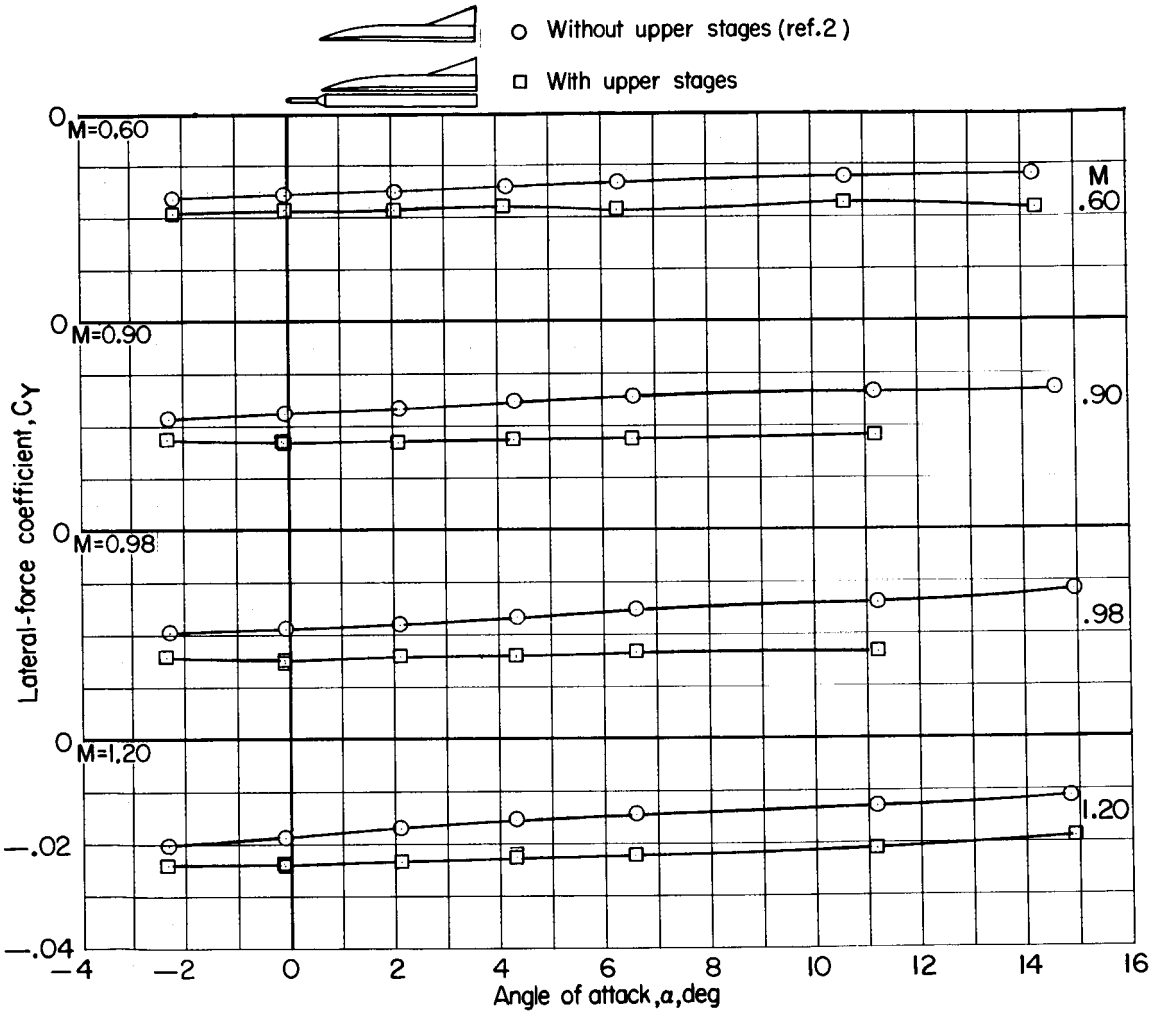

(c) Variation of side-force coefficient with angle of attack.

Figure 21.- Concluded.

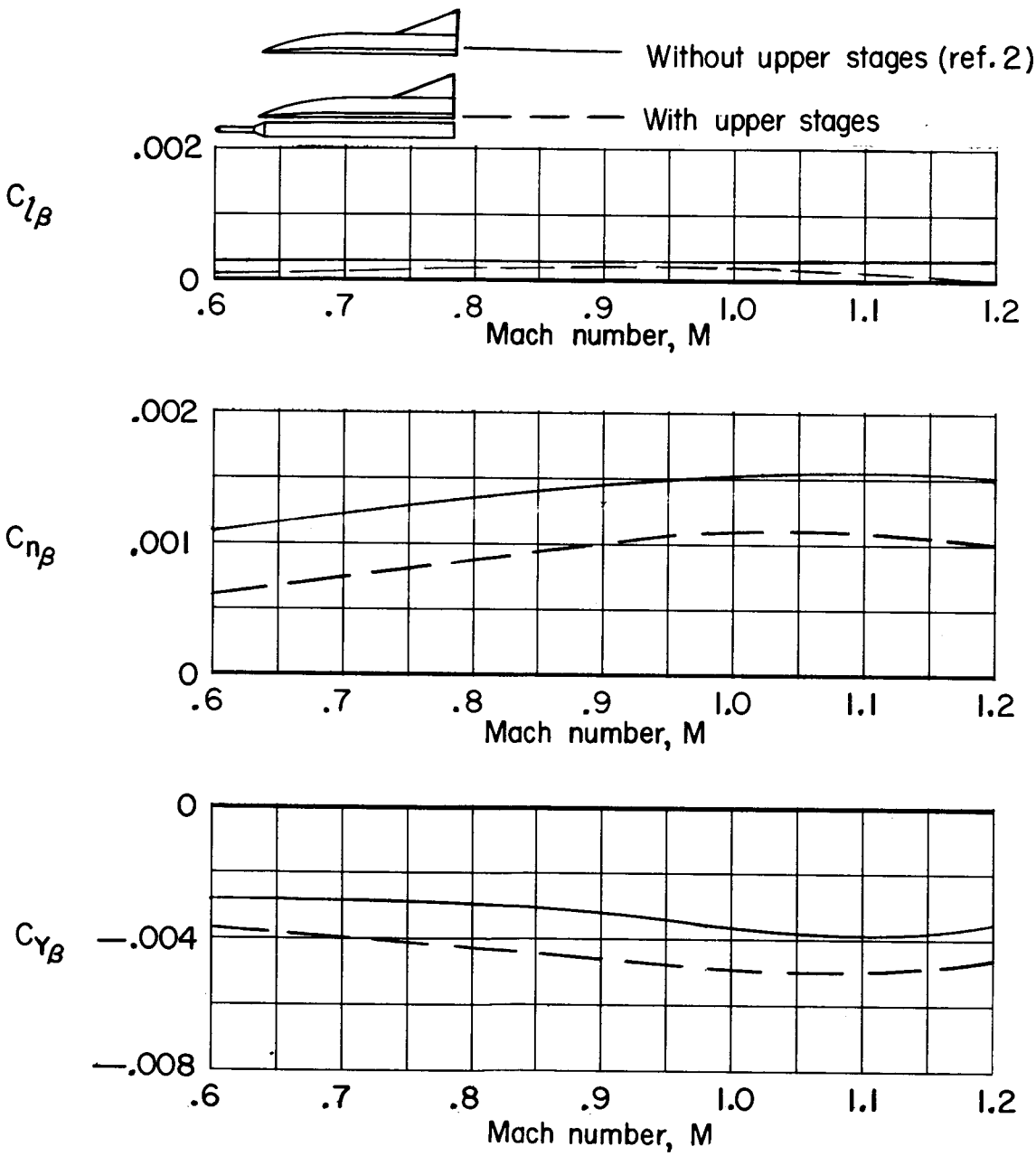

(a) $\alpha = 0^\circ$.

Figure 22.- Lateral-directional stability parameters for the low-wing recoverable booster without and with a two-stage rocket booster and winged-rocket spacecraft mounted beneath the wing.

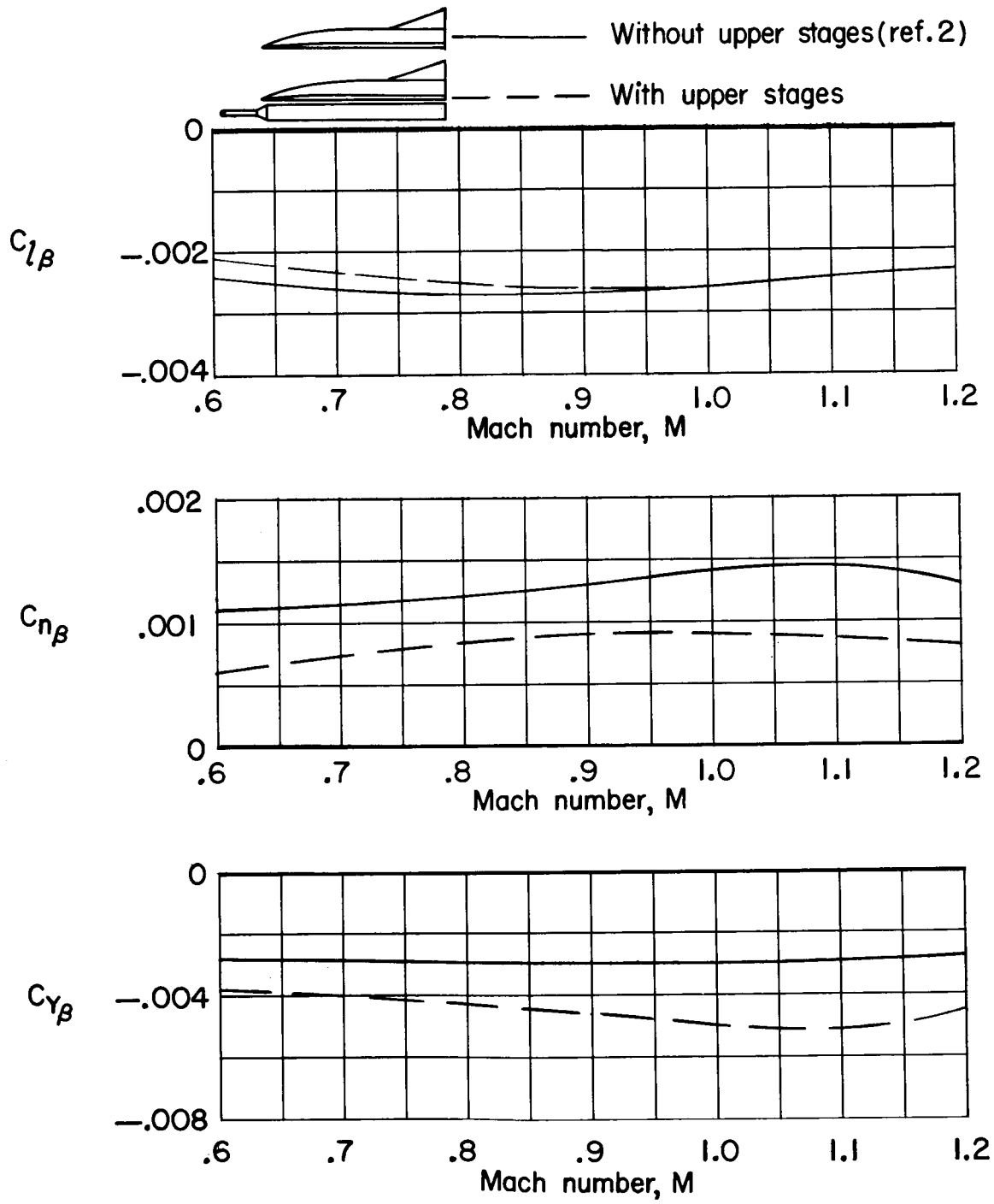

(b) $\alpha = 10^\circ$.

Figure 22.- Concluded.

L-1935